SIAM J. Applied Dynamical Systems
Vol. 11, No. 1, pp. 507–539

Bistability in a Leaky Integrate-and-Fire Neuron with a Passive Dendrite*

Michael A. Schwemmer† and Timothy J. Lewis‡

Abstract. We examine the influence of dendritic load on the firing dynamics of a spatially extended leaky integrate-and-fire (LIF) neuron that explicitly includes spiking dynamics. We obtain an exact analytical solution for this model and use it to derive a return map that completely captures the dynamics of the system. Using the map, we find that dendritic properties can significantly change the firing dynamics of the system. Under certain conditions, the addition of the dendrite can change the LIF model from type 1 excitability to type 2 excitability and induce bistability between periodic firing and the quiescent state. We identify the mechanism that causes the periodic behavior in the bistable regime as somatodendritic ping-pong. Furthermore, we use the return map to fully explore the model parameter space in order to find regions where this bistable behavior occurs. We then give physical interpretations of the dependence of the bistable behavior on model parameters. Finally, we demonstrate that the simpler two-compartment model displays qualitatively similar dynamics to the more complicated ball-and-stick model.

Key words. ball-and-stick neuronal model, bifurcation, bistability, cable equation, integrate-and-fire neuronal model, map reduction

AMS subject classifications. 34A05, 34C23, 92C05

DOI. 10.1137/110847354

1. Introduction.

Neurons are spatially extensive and heterogeneous. They typically consist of a dendritic tree, a soma (cell body), and an axon. The type of model one uses to represent a neuron depends upon a balance between mathematical tractability and biological realism and on the issue being addressed. A common technique in neuronal modeling is to represent the neuron as a single-compartment object that ignores the spatial anatomy of the cell, e.g., [11, 25, 26]. Although this simplification allows for greater mathematical tractability and computational efficiency, many neurons are not electrotonically compact. Therefore, single-compartment models cannot be expected to capture the full spectrum of electrical behavior of neurons. Dendrites can have substantial effects on the dynamics of individual neurons. For example, the architecture and ionic channel density of a dendritic tree can alter the firing pattern and encoding properties of a neuronal oscillator [19, 21, 24], while the additional electrical load due to the dendrite can alter firing frequency [36, 38]. For a full understanding of this behavior, more detailed models are required.

*Received by the editors September 8, 2011; accepted for publication (in revised form) by B. Ermentrout January 17, 2012; published electronically March 22, 2012. This work was supported by the National Science Foundation under grant DMS-0921039.
http://www.siam.org/journals/siads/11-1/84735.html
†Program in Applied and Computational Mathematics and Princeton Neuroscience Institute, Princeton University, Princeton, NJ 08544 (mschwemm@princeton.edu). While at UC Davis, this author was supported in part by NSF VIGRE grant DMS-0636297. This author is currently supported by NIH grant T32-MH065214-1 through the Princeton Neuroscience Institute.
‡Department of Mathematics, University of California-Davis, Davis, CA 95616 (tlewis@ucdavis.edu).

The branched structure of a dendritic tree can often be quite complex. However, in a series of groundbreaking papers, Rall demonstrated that each segment of a dendritic tree can be modeled as a one-dimensional cable [31, 32, 33]. Furthermore, assuming a certain relationship between the diameters of the different cables making up the tree, Rall also showed that a complicated branched dendritic tree can be reduced to a single one-dimensional cable, the so-called *equivalent cylinder* [32]. Thus, the dynamics of the membrane potential of an entire dendritic tree can be modeled using a single partial differential equation (PDE) that governs the flow of electrical activity in a one-dimensional cable. Rall's work laid the foundation for two standard approaches to modeling the electrical dynamics of neuronal dendrites. The first approach is using PDEs to either model the voltage dynamics of the dendrites between the branch points or appeal to the equivalent cylinder representation of the dendritic tree and represent it as a single one-dimensional PDE. Alternatively, the PDEs governing the voltage of the dendritic tree or equivalent cylinder can be discretized into a finite system of ordinary differential equations connected by electronic coupling (resistors) to model the neuron as a multicompartmental object, e.g., [4, 37]. Although this technique allows for greater flexibility in fitting electrophysiological data, the resulting models can be quite difficult to analyze when there is a large number of compartments. Therefore, two-compartment models are often used as a simplification of the multicompartmental approach, e.g., [23, 28]. We will utilize both the equivalent cylinder and two-compartmental approaches in this article in order to examine how dendritic properties affect the firing dynamics of neurons.

In previous work [36], we identified the mechanisms by which weak dendritic influences modulate the firing frequency of a somatic oscillator. We modeled the neuron as an isopotential somatic oscillator attached to a thin passive dendritic cable, i.e., a "ball-and-stick" model [33], and as an isopotential somatic oscillator compartment electrically coupled to a passive compartment, i.e., a two-compartment model. We made no assumption about the dynamics of the somatic oscillator, but we assumed that the dendrite was sufficiently thin so that the dynamics of the soma were only weakly perturbed. Here, we extend our previous analysis to examine the effects of nonweak dendritic influences. That is, we make no assumptions about the strength of the dendritic perturbation, but we idealize the somatic dynamics as a leaky integrate-and-fire (LIF) model that explicitly includes spike effects [6, 17, 22]. Using this framework, we seek to understand how dendritic properties alter firing dynamics. More specifically, one can characterize the firing dynamics of a neuron in response to constant current input by its frequency-applied current *f-I* curve, and we therefore examine how dendritic properties can alter the *f-I* curve of neurons. The standard LIF model [1] has an *f-I* curve typical of Hodgkin's type 1 neuronal excitability [14]; i.e., it can fire at arbitrarily low frequencies near the onset of oscillations. We find that the addition of the dendrite can change the firing dynamics of the standard LIF model to Hodgkin's type 2 excitability (the onset of periodic oscillations occurs with a nonzero frequency) and cause the system to display bistability between periodic firing and the quiescent state, allowing the cell to now behave like a neuronal switch. In this bistable regime, the periodic behavior arises from a "ping-pong" effect [2, 39] between the somatic and proximal dendritic membrane potentials. We then examine how altering system parameters affects the presence of this bistability. Finally, we demonstrate that the same qualitative behavior is captured in the simpler two-compartment model.

The paper is organized as follows. In section 2, we describe the LIF ball-and-stick model. Section 3 illustrates how the analytical solution for this model can be obtained and used to derive a return map that captures the dynamics of the system. In section 4 we show that, under certain conditions, the model can exhibit bistable behavior between periodic firing and quiescence, and we discuss the mechanisms that lead to this bistability. The parameter space of the system is then probed using two different functions describing the somatic dynamics during the spike. Sections 5 and 6 present the two-compartment LIF model and the derivation of its one-dimensional return map that captures the system's dynamics, respectively. In section 7 we show that the dynamics of the two-compartment model are qualitatively similar to the ball-and-stick model. The paper then closes with a discussion in section 8 where we discuss the relevance of our results and their relationship to previous studies. Finally, we include an appendix in which we show that the addition of point source dendritic inputs quantitatively, but not qualitatively, affects the results of the main paper.

2. LIF ball-and-stick model. We model a neuron as an isopotential spherical soma attached to a passive dendrite, i.e., a ball-and-stick model [8]. The dendrite is modeled as a one-dimensional passive cable of length ℓ using the cable equation [31, 32, 33]

$$C_m \frac{\partial \overline{V}}{\partial \overline{t}} = \frac{a}{2R_c} \frac{\partial^2 \overline{V}}{\partial \overline{x}^2} - g_{LD}(\overline{V} - E_{LD}), \quad 0 < \overline{x} < \ell, \tag{2.1}$$

where $\overline{V}(\overline{x}, \overline{t})$ is the membrane potential of the cable at position $\overline{x}$ and time $\overline{t}$, C_m is the membrane capacitance, g_{LD} is the dendritic leakage conductance, E_{LD} is the reversal potential of the dendritic leakage current, R_c is the cytoplasmic resistivity, and a is the radius of the dendrite. Note that the cable can be thought of as a single dendrite or as the equivalent cylinder of a branched dendritic structure [32, 34].

No current is assumed to pass through the distal end, $\overline{x} = \ell$, of the dendrite, resulting in the boundary condition

$$\frac{\partial \overline{V}}{\partial \overline{x}}(\ell, \overline{t}) = 0. \tag{2.2}$$

The boundary condition at $\overline{x} = 0$ is provided by the somatic dynamics and an application of Kirchhoff's law of current conservation. The isopotential soma is modeled as an LIF neuron that explicitly includes a spike (i.e., an action potential) [6, 17, 22]. The boundary condition at $\overline{x} = 0$ for the "nonspike" portion of the model is described by

$$C_m \frac{\partial \overline{V}}{\partial \overline{t}}(0, \overline{t}) = -g_L(\overline{V}(0, \overline{t}) - E_L) + \overline{I} + \frac{a^2}{d^2 R_c} \frac{\partial \overline{V}}{\partial \overline{x}}(0, \overline{t}), \tag{2.3}$$

where g_L is the somatic leakage conductance, E_L is the somatic leakage reversal potential, d is the diameter of the soma, and $\overline{I}$ is a constant current applied to the soma. Changes in E_{LD} can be interpreted as arising from constant input to the dendrites. Note that (2.1)–(2.3) describe the Rall lumped soma model.

If the somatic membrane potential increases to a threshold potential of $\overline{V}_{th}$ at time $\overline{t}$, a somatic spike is elicited. If this is the jth spike that has occurred, we set the jth firing time

Table 1
List of all model parameters.

Parameters			
C_m	membrane capacitance	g_L	somatic leakage conductance
a	dendritic radius	E_L	somatic leakage reversal potential
R_c	cytoplasmic resistivity	$\overline{I}$	somatic bias current
g_{LD}	dendritic leakage conductance	$\overline{V}_{th}$	somatic threshold potential
E_{LD}	dendritic leakage reversal potential	$\overline{V}_R$	somatic reset potential
ℓ	length of the dendrite	$\overline{t}_S^j$	jth somatic spike time
d	somatic diameter	$\overline{T}_a$	duration of the somatic spike

to be $\overline{t}_s^j = \overline{t}$ and change the boundary condition at $\overline{x} = 0$ to the "spike" boundary conditions for the duration of the spike

$$\overline{V}(0,\overline{t}) = \overline{h}(\overline{t} - \overline{t}_s^j), \qquad \overline{t} \in (\overline{t}_s^j, \overline{t}_s^j + \overline{T}_a], \tag{2.4}$$

where $\overline{h}(\overline{t})$ is a function that describes the shape of the spike, and $\overline{T}_a$ is the duration of the spike. At time $\overline{t} = \overline{t}_s^j + \overline{T}_a$, the boundary condition at $\overline{x} = 0$ is set back to (2.3), which gives an effective reset potential of $\overline{h}(\overline{T}_a)$. For reference, Table 1 lists the definitions of all of our model parameters.

In nondimensional form, the full LIF ball-and-stick model that incorporates spiking dynamics is given by

$$\frac{\partial V}{\partial t} = \frac{\partial^2 V}{\partial x^2} - V, \tag{2.5}$$

$$\begin{cases} V(0,t) = h(t - t_s^j) & \text{if } t \in (t_s^j, t_s^j + T_a] \quad \text{[spike]}, \\ \dfrac{\partial V}{\partial t}(0,t) = -G_L V(0,t) + I + \gamma \dfrac{\partial V}{\partial x}(0,t) & \text{if } t \in (t_s^j + T_a, t_s^{j+1}] \quad \text{[nonspike]}, \end{cases} \tag{2.6}$$

$$\frac{\partial V}{\partial x}(L,t) = 0, \tag{2.7}$$

$$V(x, t_s^j) = V^j(x), \tag{2.8}$$

where $V = V(x,t) = \frac{\overline{V}(\overline{x}/\lambda, \overline{t}/\tau_D) - E_{LD}}{\overline{V}_{th} - E_{LD}}$, $\lambda = \sqrt{\frac{a}{2R_c g_{LD}}}$ is the space constant of the dendrite, $\tau_D = C_m/g_{LD}$ is the time constant of the dendrite, $t = \overline{t}/\tau_D$, $t_s^j = \overline{t}_s^j/\tau_D$, $T_a = \overline{T}_a/\tau_D$, $h(t) = \frac{\overline{h}(\overline{t}) - E_{LD}}{\overline{V}_{th} - E_{LD}}$, $x = \frac{\overline{x}}{\lambda}$, $L = \frac{\ell}{\lambda}$ is the electrotonic length of the dendrite, $V_{th} = \frac{\overline{V}_{th} - E_{LD}}{\overline{V}_{th} - E_{LD}} = 1$ is the nondimensionalized threshold potential, and

$$\gamma = \frac{a^2}{d^2 R_c g_{LD} \lambda}, \tag{2.9}$$

$$G_L = g_L/g_{LD}, \tag{2.10}$$

$$I = \frac{\overline{I} + g_L(E_L - E_{LD})}{g_{LD}(\overline{V}_{th} - E_{LD})}. \tag{2.11}$$

The parameter γ sets the magnitude of the perturbation to the somatic dynamics caused by the dendrite.

The above model can display two types of stable characteristic behavior depending on parameters: (i) time-independent steady-states, and (ii) steady periodic oscillations.

3. Derivation of return map for the LIF ball-and-stick neuron model. In this section, we construct an analytical solution for the spatially extended LIF model (2.5)–(2.8). The solution maps the voltage profile along the model neuron at the onset of the jth spike ($V(x,t_s^j)=V^j(x)$) to the voltage profile at the onset of the $j+1$st spike ($V(x,t_s^{j+1})=V^{j+1}(x)$). Thus, it takes the form of a return map that can be iterated to capture the full dynamics of the system. The solution is constructed by piecing together the solution for the case when the soma is spiking and the solution for the case when it is not spiking. First, we solve the system (2.5)–(2.8) with the "spike" boundary condition at the soma $x=0$ and the initial condition $V(x,t_s^j)=V^j(x)$ and evaluate this solution at the end of the spike to obtain $V(x,t_s^j+T_a)$. We then switch to the "nonspike" boundary condition at the soma and solve system (2.5)–(2.8), using $V(x,t_s^j+T_a)$ as the initial condition. Finally, we find the time t_s^{j+1} at which the somatic membrane potential reaches the threshold potential and initiates a new spike and evaluate the corresponding voltage profile along the neuron at this time. This yields $V(x,t_s^{j+1})=V^{j+1}(x)$.

3.1. Spike solution. We assume that the model neuron reaches threshold and the jth spike is initiated at time t_s^j. Therefore, we consider the system (2.5)–(2.8) with the spike boundary condition at the soma $x=0$, the no-flux distal boundary condition at $x=L$, and the initial condition $V(x,t_s^j)=V^j(x)$. To obtain the solution over the duration of the spike (i.e., from time t_s^j to $t_s^j+T_a$), we introduce the change of variables

$$V(x,t)=U(x,t)+h(t-t_s^j)\tilde{V}^{ss}(x), \tag{3.1}$$

where $\tilde{V}^{ss}$ is the steady state solution of (2.5)–(2.8) with the somatic boundary condition set to $V(0,t)=1$, i.e.,

$$\tilde{V}^{ss}(x)=\frac{\cosh(L-x)}{\cosh(L)}, \tag{3.2}$$

and $U(x,t)$ solves the system

$$\begin{aligned}
&\frac{\partial U}{\partial t}=\frac{\partial^2 U}{\partial x^2}-U-h'(t-t_s^j)\tilde{V}^{ss},\\
&U(0,t)=0,\\
&\frac{\partial U}{\partial x}(L,t)=0,\\
&U(x,t_s^j)=V^j(x)-h(0)\tilde{V}^{ss}(x).
\end{aligned}$$

Separation of variables can be used to find $U(x,t)$. This yields the solution for the neuronal model during the spike in the form of an eigenfunction expansion

$$\begin{aligned}
V(x,t)=&\sum_{m=0}^{\infty}\left(\tilde{V}_m^j+\tilde{V}_m^{ss}q_m(t-t_s^j)\right)e^{-(1+\lambda_m^2)(t-t_s^j)}Y_m(x)\\
&+h(t-t_s^j)\tilde{V}^{ss}(x),\quad t\in[t_s^j,t_s^j+T_a),
\end{aligned} \tag{3.3}$$

where

$$Y_m(x) = \cos(\lambda_m(L-x)), \tag{3.4}$$

and

$$\lambda_m = \frac{(2m+1)\pi}{2L},$$
$$q_m(t) = \int_0^t h'(s)e^{(1+\lambda_m^2)s}ds - h(0),$$
$$\tilde{V}_m^j = \frac{\langle V^j(x), Y_m(x)\rangle}{\langle Y_m(x), Y_m(x)\rangle},$$
$$\tilde{V}_m^{ss} = \frac{\langle \tilde{V}^{ss}(x), Y_m(x)\rangle}{\langle Y_m(x), Y_m(x)\rangle} = \frac{2(-1)^m\lambda_m}{(1+\lambda_m^2)L}.$$

Note that the eigenfunctions $Y_m(x)$ are orthogonal under the standard L_2 inner product on $0 \le x \le L$, i.e., $\langle Y_n(x), Y_m(x)\rangle = 0$ for $n \ne m$, and thus the series representation of the solution is guaranteed to converge owing to Parseval's identity.

Thus, the membrane potential along the neuron at the end of the jth spike is

$$V^{j+\frac{1}{2}}(x) = V(x, t_s^j + T_a) = \sum_{m=0}^{\infty} \tilde{V}_m^{j+\frac{1}{2}} Y_m(x), \tag{3.5}$$

where

$$\tilde{V}_m^{j+\frac{1}{2}} = \left(\tilde{V}_m^j + q_m(T_a)\tilde{V}_m^{ss}\right) e^{-(1+\lambda_m^2)T_a} \; + \; h(T_a)\tilde{V}_m^{ss}.$$

It will be convenient to express this solution as a map that takes $\overrightarrow{\tilde{V}}^j = [\tilde{V}_m^j]_{m=0}^{\infty}$ (the vector of coefficients for the expansion of $V^j(x)$ in terms of the eigenfunctions $Y_m(x)$) to $\overrightarrow{\tilde{V}}^{j+\frac{1}{2}} = [\tilde{V}_m^{j+\frac{1}{2}}]_{m=0}^{\infty}$ (the vector of the eigenfunction expansion coefficients of $V^{j+\frac{1}{2}}(x)$)

$$\Phi_Y^S : \overrightarrow{\tilde{V}}^j \to \overrightarrow{\tilde{V}}^{j+\frac{1}{2}} = \Omega^S \; \overrightarrow{\tilde{V}}^j + (\Omega^S Q + H) \; \overrightarrow{\tilde{V}}^{ss}, \tag{3.6}$$

where Q, H, and Ω^S are diagonal matrices with elements

$$Q_{mm} = q_m(T_a), \tag{3.7}$$
$$\Omega_{mm}^S = e^{-(1+\lambda_m^2)T_a}, \tag{3.8}$$
$$H_{mm} = h(T_a). \tag{3.9}$$

3.2. Nonspike solution. To obtain the solution of the neuronal model (2.5)–(2.8) in between the jth spike and the $j+1$st spike, we consider the system (2.5)–(2.8) with the nonspike boundary condition at the soma $x = 0$, the no-flux distal boundary condition at $x = L$, using the voltage profile along the dendrite at the end of the jth spike as the initial condition $V(x, t_s^j + T_a) = V^{j+\frac{1}{2}}(x)$. The solution can be decomposed into a steady-state portion $V^{ss}(x)$ and a time-dependent portion $W(x,t)$,

$$V(x,t) = W(x,t) + V^{ss}(x). \tag{3.10}$$

The steady-state portion of the nonspike solution is

$$V^{ss}(x) = \rho \cosh(L - x), \tag{3.11}$$

where

$$\rho = \frac{I}{\gamma \sinh(L) + G_L \cosh(L)}.$$

The time-dependent portion of solution $W(x,t)$ can be found by using separation of variables, which yields $W(x,t)$ in the form of an eigenfunction expansion

$$W(x,t) = \sum_{n=0}^{\infty} A_n e^{-(1+\alpha_n^2)t} X_n(x), \tag{3.12}$$

where

$$X_n(x) = \cos(\alpha_n(L - x)) \tag{3.13}$$

are eigenfunctions and the corresponding eigenvalues α_n are the solutions to the transcendental equation

$$\alpha_n \gamma = [G_L - (1 + \alpha_n^2)] \cot(\alpha_n L). \tag{3.14}$$

Note that (3.14) has an infinite number of isolated solutions (Figure 1). Because the eigenfunctions $X_n(x)$ are even, we need only consider positive α_n.

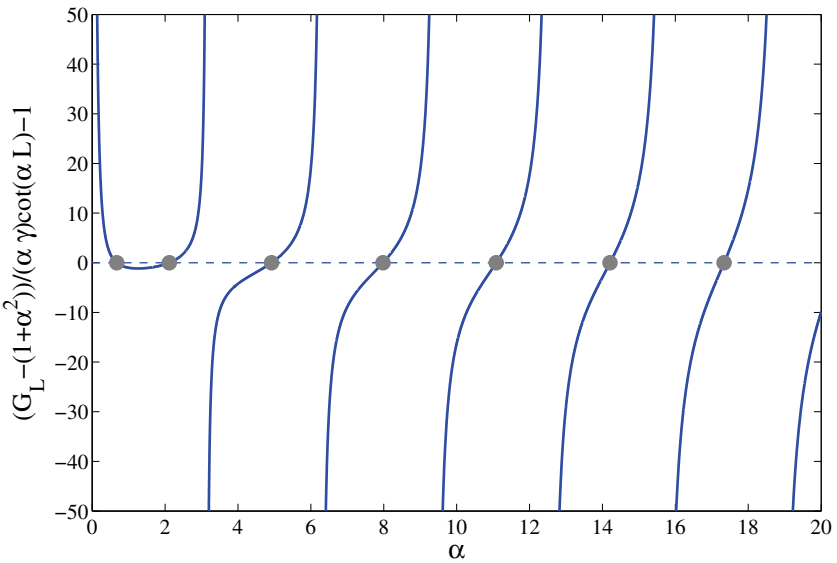

Figure 1. Graphical representation of the eigenvalues α_n. *There is an infinite number of solutions* α_n *that are given by the solutions of* (3.14). *The solid line plots* $[G_L - (1 + \alpha_n^2)] \cot(\alpha_n L) - \alpha_n \gamma$, *and the dashed line is the zero line.*

The coefficients A_n in (3.12) are determined by applying the initial condition corresponding to the membrane potential along the neuron at the end of the jth spike (i.e., at $t = t_s^j + T_a$; see (3.5)),

$$V(x, t^j + T_a) = V^{j+\frac{1}{2}}(x) = \sum_{n=0}^{\infty} A_n e^{(1+\alpha_n^2)[t_s^j + T_a]} \cos(\alpha_n(L-x)) + V^{ss}(x).$$

To compute the coefficients A_n, the steady-state solution $V^{ss}(x)$ and initial condition $V^{j+\frac{1}{2}}(x)$ must be expanded in terms of the eigenfunctions $X_n(x)$. Due to the boundary conditions at the soma ($x = 0$), $X_n(x)$ are not orthogonal under the standard L_2 inner product on $0 \le x \le L$ (unless $\gamma = 0$). Therefore, we define a modified L_2 inner product under which $X_n(x)$ are orthogonal [7, 10]

$$\langle f, g \rangle_A = \int_0^L f(x)\ g(x)\ dx + \frac{1}{\gamma}\ f(0)\ g(0), \tag{3.15}$$

i.e., $\langle X_n(x), X_m(x) \rangle_A = 0$ for $n \neq m$. Using this modified inner product, we can write the subthreshold solution of the neuronal model between the end of the jth spike and the beginning of the $j+1$st spike as

$$V(x,t) = \sum_{n=0}^{\infty} (V_n^{j+\frac{1}{2}} - V_n^{ss}) e^{-(1+\alpha_n^2)[t-(t_s^j+T_a)]} X_n(x) + V^{ss}(x), \qquad t \in [t_s^j + T_a, t_s^{j+1}), \tag{3.16}$$

where

$$\begin{aligned} V_n^{j+\frac{1}{2}} &= \frac{\left\langle V^{j+\frac{1}{2}}(x), X_n(x) \right\rangle_A}{\langle X_n(x), X_n(x) \rangle_A}, \\ V_n^{ss} &= \frac{\langle V^{ss}(x), X_n(x) \rangle_A}{\langle X_n(x), X_n(x) \rangle_A} \\ &= \frac{\alpha_n^2}{1+\alpha_n^2} \frac{(2X_n(0))(I - \alpha_n^2 V^{ss}(0))}{L\gamma\alpha_n^2 + (G_L - (1-\alpha_n^2))(X_n(0))^2} \qquad \text{for } \alpha_n \neq 0. \end{aligned} \tag{3.17}$$

For the special case of $\alpha_k = 0$, $V_k^{ss} = I/(\gamma L + 1)$; this case occurs only when $G_L = 1$. Note that, like the spiking case, the series representation of the solution of the nonspiking portion of the model is of the form of an eigenfunction expansion and is also guaranteed to converge [7].

The $j+1$st spike time and the corresponding jth interspike interval $\Delta t_s^j = t_s^{j+1} - t_s^j$ are obtained by setting the somatic membrane potential in (3.16) to threshold ($V_{th} = 1$) and finding the smallest positive solution of the resulting transcendental equation

$$V(0, t_s^{j+1}) = \sum_{n=0}^{\infty} ((V_n^j - V_n^{ss}) e^{-(1+\alpha_n^2)[\Delta t_s^j - T_a]} + V_n^{ss}) \cos(\alpha_n L) = 1. \tag{3.18}$$

If no solution to this equation exists, then the interspike interval Δt_s^j is taken to be infinity, i.e., the model neuron does not fire again and asymptotically approaches the time-independent steady-state $V^{ss}(x)$.

Thus, the membrane potential along the neuron at the initiation time of the $j+1$st spike is

$$V^{j+1}(x) = V(x, t_s^{j+1}) = \sum_{n=0}^{\infty} V_n^{j+1} X_n(x), \tag{3.19}$$

where

$$V_n^{j+1} = (V_n^j - V_n^{ss}) e^{-(1+\alpha_n^2)[\Delta t_s^j - T_a]} + V_n^{ss}.$$

We can express the nonspike solution as a map that takes $\overrightarrow{V}^{j+\frac{1}{2}} = [V_n^{j+\frac{1}{2}}]_{n=0}^{\infty}$ (the vectors of coefficients of the expansion of $V^{j+\frac{1}{2}}(x)$ in terms of the eigenfunctions $X_n(x)$) to $\overrightarrow{V}^{j+1} = [V_n^{j+1}]_{n=0}^{\infty}$ (the vectors of coefficients of the expansion of $V^{j+1}(x)$),

$$\Phi_X^{NS} : \overrightarrow{V}^{j+\frac{1}{2}} \to \overrightarrow{V}^{j+1} = \Omega^{NS,j} \, (\overrightarrow{V}^{j+\frac{1}{2}} - \overrightarrow{V}^{ss}) + \overrightarrow{V}^{ss}, \tag{3.20}$$

where $\Omega^{NS,j}$ is a diagonal matrix with elements

$$\Omega_{nn}^{NS,j} = e^{-(1+\alpha_n^2)(\Delta t_s^j - T_a)}. \tag{3.21}$$

3.3. The return map. By combining the map defined for the spike portion of the solution $\Phi_Y^S : \overrightarrow{V}^j \to \overrightarrow{V}^{j+\frac{1}{2}}$ and the map defined for the nonspike portion of the solution $\Phi_X^{NS} : \overrightarrow{V}^{j+\frac{1}{2}} \to \overrightarrow{V}^{j+1}$, we obtain a map that takes the membrane potential along the neuron at the end of the jth spike, $V^j(x)$, to the membrane potential along the neuron at the end of the $j+1$st spike, $V^{j+1}(x)$. However, the solutions for the spike and nonspike portions are expanded in different sets of basis functions. Therefore, before composing the maps, we first change the basis for the map for the spike portion of the solution Φ_Y^S (3.6), so that coefficients correspond to expansions of the membrane potentials in $X_n(x)$ rather than $Y_n(x)$,

$$\Phi_X^S : \overrightarrow{V}^j \to \overrightarrow{V}^{j+\frac{1}{2}} = P\Omega^S R \, \overrightarrow{V}^j + P(\Omega^S Q + H) R \, \frac{\overrightarrow{V}^{ss}}{V^{ss}(0)}, \tag{3.22}$$

where the factor of $1/V^{ss}(0)$ comes from the relation $\tilde{V}^{ss} = \frac{V^{ss}}{V^{ss}(0)}$ (see (3.2)) and the elements of the "change of basis" matrices are

$$\begin{aligned} P_{mn} &= \frac{\langle Y_m(x), X_n(x) \rangle_A}{\langle X_n(x), X_n(x) \rangle_A} \\ &= \frac{(-1)^n \frac{4\pi\gamma(2n+1)L}{((2n+1)\pi)^2 - (2\alpha_n L)^2} + 2\cos(\frac{(2m+1)}{2}\pi)}{\cos(\alpha_n L)(\beta_n + \gamma L/\cos^2(\alpha_n L) + 2)}, \\ R_{mn} &= \frac{\langle X_n(x), Y_m(x) \rangle}{\langle Y_m(x), Y_m(x) \rangle} \\ &= \frac{2(-1)^m \lambda_m}{(\lambda_m^2 - \alpha_n^2)L} \cos(\alpha_n L). \end{aligned}$$

The full map is then

$$\Phi_X = \Phi_X^S \circ \Phi_X^{NS} : \overrightarrow{V}^{j+1} = \Omega^{NS,j} P \Omega^S R \, \overrightarrow{V}^j + \Omega^{NS,j} \left[P(\Omega^S Q + H) R - \mathbb{I} \right] \frac{\overrightarrow{V}^{ss}}{V^{ss}(0)} + \overrightarrow{V}^{ss}, \tag{3.23}$$

where Q, H, and Ω^S are given in (3.7)–(3.8), $\Omega^{NS,j}$ is given in (3.21), and $\mathbb{I}$ is the identity matrix.

This infinite dimensional map takes $V^j(x)$ to $V^{j+1}(x)$ in terms of their expansion coefficients of the eigenfunctions $X_n(x)$ (Figure 2). The matrices in the map capture all filtering effects of the dendrite and the effects of the somatic spike. By iterating this map, the dynamics of the full ball-and-stick neuronal model can be assessed. Note, however, that while the map (3.23) itself is linear, each iteration involves solving the scalar transcendental equation (3.18) for interspike interval Δt_s^j, which is needed to evaluate $\Omega^{NS,j}$. Thus, the entire map is nonlinear. Fixed points of this map correspond to either periodic oscillations or quiescent behavior. However, if (3.18) has no solution, the interspike interval Δt_s^j is infinity and $\Omega^{NS,j}$ is the zero matrix. In this case, the map takes $\overrightarrow{V}^j$ to $\overrightarrow{V}^{ss}$, which corresponds to the time-independent steady-state of the nonspike solution $V^{ss}(x)$.

In the next section, we use the map to probe the neuronal model's behavior. Although the solution is in the form of an infinite series, the coefficients V_n^j decay rapidly as n is increased. Therefore, we truncate the series to include the first 10 terms. To check the accuracy of the truncated series, we performed direct numerical simulations of the model (2.5)–(2.8) using a Crank–Nicolson method and found that the two solutions were in excellent agreement.

4. Dynamics of the spatially extended LIF neuron model. In this section, we describe the behavior of the LIF ball-and-stick neuron model that was found by analyzing the map derived in the previous section. Two different functions are used to approximate the shape of the spike, $h(t)$: a "sigmoidal" spike and a "linear" spike. We determine the parameter values at which the time-independent "quiescent" steady-state ceases to exist and the parameter values at which stable periodic oscillations appear. We find that the system can display bistability between periodic firing and quiescence, and we examine how altering various parameters affects the region of parameter space where bistability exists. Note that the bistability described here is not possible in the standard LIF model [1] nor in spatially extended LIF models that do not explicitly include spikes [3, 21].

4.1. The quiescent steady-state. Recall that the steady-state voltage of the ball-and-stick LIF neuron with the nonspiking proximal boundary condition is given by (3.11). Using this equation, one can determine the amount of current needed to bring the steady-state membrane potential of the soma to threshold ($V_{ss}(x=0)=1$)

$$I_{th} = G_L + \gamma \tanh(L). \tag{4.1}$$

If the current applied to the soma is less than this threshold current ($I < I_{th}$), then there exists a time-independent voltage profile given by (3.11), i.e., the quiescent steady-state. On the other hand, if $I > I_{th}$, then the steady-state voltage of the soma would be above the threshold voltage of 1. This implies that the quiescent steady-state does not exist and the soma will fire repetitively. Note that, because $V_{th} = 1$, I_{th} is equal to the nondimensional input conductance of the model neuron at the soma [18]. Also, note that the equation for the threshold current, (4.1), separates the influences of the passive properties of LIF soma (G_L) from those of the dendritic load ($\gamma \tanh(L)$). Furthermore, as $\gamma \to 0$ or $L \to 0$, then I_{th} approaches the value that would be obtained for the standard LIF model.

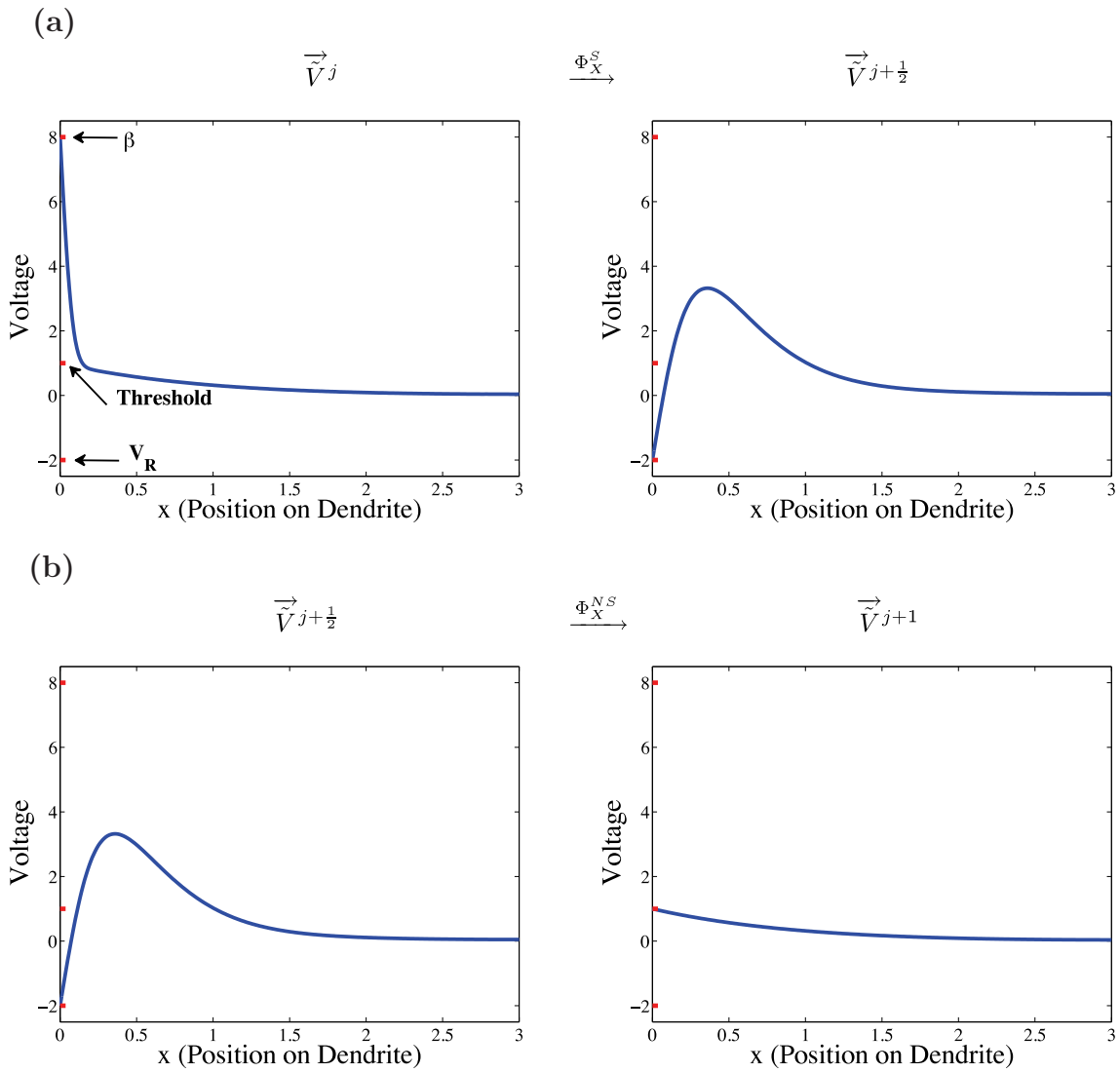

Figure 2. Return map for the LIF ball-and-stick model. (a) Φ_X^S *maps the coefficients of eigenfunction expansion of the dendritic voltage at the beginning of the* j*th somatic spike* ($V^j(x)$*; shown on left) to coefficients of the voltage profile at the end of the* j*th somatic spike when the somatic potential is reset to* V_R ($V^{j+\frac{1}{2}}(x)$*; shown on right). For illustrative purposes, in the left figure, we show the voltage profile soon after the soma has jumped to the value* β *rather than exactly at the onset of the somatic spike.* (b) Φ_X^{NS} *maps the coefficients of eigenfunction expansion of the dendritic voltage from the end of the* j*th somatic spike* ($V^{j+\frac{1}{2}}(x)$*; shown on left) to coefficients of the voltage profile at the onset of the* $j+1$*st spike, i.e., the voltage profile when the the somatic voltage has reached threshold* ($V^{j+1}(x)$*; shown on right). The composition of the two maps* $\Phi_X = \Phi_X^{NS} \circ \Phi_X^S$ *effectively maps the membrane potential along the neuron at the onset of the* j*th spike,* $V^j(x)$*, to the membrane potential along the neuron at the onset of the* $j+1$*st spike,* $V^{j+1}(x)$*.*

4.2. The sigmoidal spike. For the case of the "sigmoidal" spike, the somatic membrane potential is instantaneously increased to a value β when the voltage at the soma reaches

threshold. The somatic membrane potential then decreases very slowly until a time $t \sim T_a$ when the somatic voltage is quickly, but smoothly, repolarized to a value of V_R (see Figure 3). The functional form of the sigmoidal spike is

$$h(t) = \beta(1 - e^{p(t-T_a)})^4 + V_R(1 - (1 - e^{p(t-T_a)})^4), \quad t \in (0, T_a], \tag{4.2}$$

where β represents the maximal somatic potential during the spike, T_a is the duration of the spike, V_R is the value of the somatic potential at the end of the spike, and p controls the rate of repolarization of the spike. We set $p = 80$ in all of the figures shown. Note that the function $h(t)$ converges to the Heaviside function as $p \to \infty$. Thus, the sigmoidal spike can be thought of as a continuous approximation to a box function.

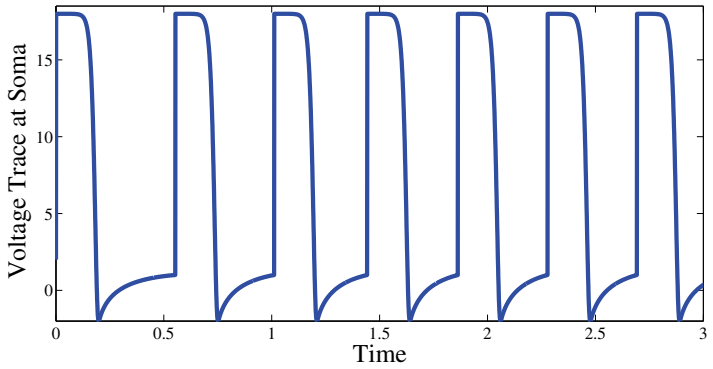

Figure 3. Voltage trace at the soma ($x = 0$) with the "sigmoidal" spike function (see (4.2)). *The sigmoidal spike abruptly increases the somatic voltage to a value β, maintains the somatic voltage near this value at time $\sim T_a$, and then quickly, but smoothly, resets the somatic voltage to a value of V_R. The parameters used in this example are $\beta = 18$, $T_a = 0.2$, $V_R = -2$, $p = 80$, $I = 2$, $\gamma = 1$, $L = 1$, and $G_L = 2$.*

4.2.1. *f-I* curves, bistability, and somatodendritic ping-pong. The frequency-applied current (*f-I*) curve for the standard LIF neuron, which corresponds to $\gamma = 0$ in our model, is plotted in Figure 4 (a) for $G_L = 2$. In accordance with (4.1), the stable quiescent steady-state exists only for applied currents I less than $I_{th} = G_L$, and the neuron fires periodically for applied currents above this value. The *f-I* curve monotonically increases from zero as I is increased. The ability to fire at arbitrarily low frequencies near the onset of oscillations is characteristic of Hodgkin's type 1 neuronal excitability [14].

Figure 4 (b) shows an example of an *f-I* curve in which the dendrite is included ($\gamma = 1$). As expected from (4.1), the stable quiescent steady-state exists for $I < I_{th} \approx 3$, and the neuron fires periodically when $I > I_{th}$. However, unlike the standard LIF neuron, the oscillatory regime also extends backward beyond I_{th}. That is, the addition of the dendrite gives rise to a region of bistability between periodic firing and a stable quiescent steady-state. Furthermore, the neuron model cannot fire at arbitrarily low frequencies. Instead, it has a minimum nonzero frequency at the onset of oscillations, which is characteristic of neurons with Hodgkin's type 2 excitability.

The repetitive firing of the neuron model when $I < I_{th}$ (as seen in Figure 4 (b)) results from a ping-pong action between the somatic and dendritic membrane potentials [2, 39]. This

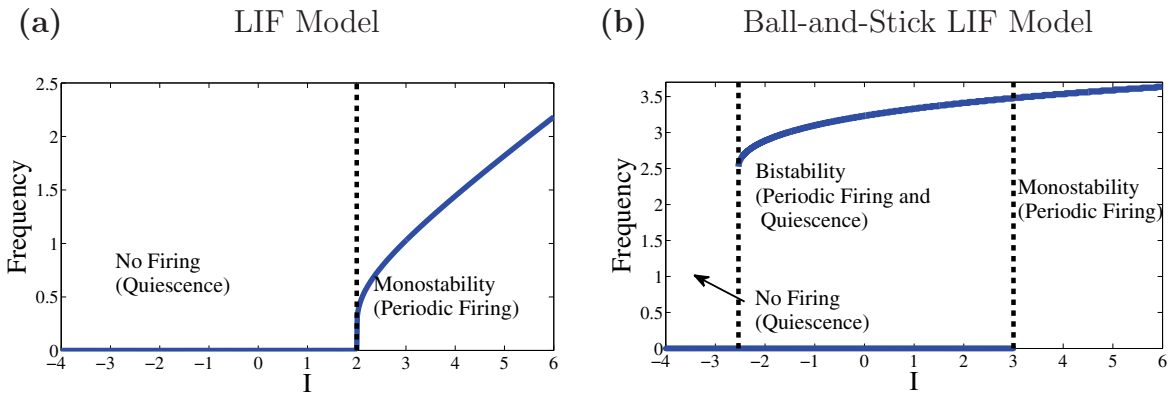

Figure 4. Addition of the dendrite causes bistability in the LIF neuron. (a) *Frequency-applied current (f-I) curve for the standard LIF neuron ($\gamma = 0$ in our model) for $G_L = 2$ and $V_R = -2$. For $I < I_{th} = 2$, there is a globally stable quiescence steady-state. For $I > I_{th}$, the quiescence steady-state does not exist and the neuron fires periodically.* (b) *Frequency-applied current curve for the LIF ball-and-stick model with $\beta = 28$, $T_a = 0.2$, $V_R = -2$, $\gamma = 1$, $L = 3$, and $G_L = 2$. For these parameters, a stable quiescent steady-state voltage exists, $I < I_{th} \approx 3$, and the neuron fires periodically for $I > I_{th}$. However, there is a range of I below I_{th} for which periodic activity stably coexists with the quiescent steady-state.*

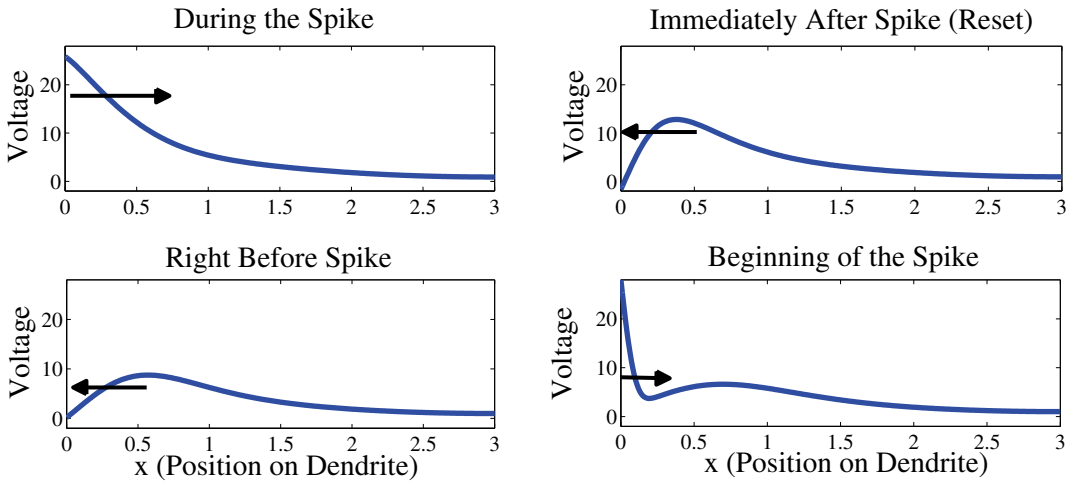

Figure 5. Voltage traces of the dendrite at different times during the cycle illustrating somatodendritic ping-pong for the sigmoidal spike. *During the somatic spike, the dendrite is depolarized to a large enough potential so that, when the somatic potential is reset, the potential difference between the soma and proximal dendrite causes a depolarizing current to flow into the soma. This current brings the soma back above threshold even though the applied current is below I_{th}. The parameters used in this simulation are $L = 3$, $G_L = 2$, $\gamma = 1$, $I = 1.5$, $\beta = 28$, $V_R = -2$, and $T_a = 0.2$. Note that for these parameter values, $I_{th} \simeq 3$. The arrows indicate the direction of depolarizing current flow between the soma and the dendrite.*

ping-pong effect can be explained by examining the spatial voltage profiles at different times during the cycle (Figure 5). During the spike, the portion of the dendrite proximal to the

soma becomes so depolarized that, once the soma repolarizes, the gradient of the membrane potential between the soma and proximal dendrite causes a large depolarizing current to flow into the soma. This current from the dendrite brings the membrane potential of the soma back to threshold even when the current applied to the soma alone is insufficient to bring the steady-state somatic potential to threshold (i.e., $V^{ss}(0) < V_{th}$).

Note that repetitive firing of ping-pong spikes can occur only if conditions are such that $V(0,t)$ overshoots $V^{ss}(0)$ and $V^{ss}(0)$ is sufficiently close to V_{th}. Whether or not the overshoot occurs depends critically on both the spike parameters and the passive neuron properties. These are in turn determined by both the spike parameters and the passive neuron properties. Below we explore the parametric dependence of the existence of the quiescent steady-state and oscillations via the ping-pong effect.

4.2.2. Effects of parameters on the region of bistability. Figures 6 and 7 show two parameter bifurcation diagrams for the current applied to the soma I, (2.11), versus the spike parameters (β, T_a) and the passive neuron properties (G_L, γ, L), respectively. Solid and dashed curves partition parameter space into a regime in which only a stable quiescent steady-state exists (no firing), a regime in which only stable periodic oscillations exist (monostability), and a regime in which both a stable quiescent steady-state and stable periodic oscillations exist (bistability).

The solid lines represent I_{th}, the value of the applied current above which the quiescent steady-state does not exist and oscillations are guaranteed to exist. I_{th} is determined directly from (4.1). Because I_{th} is determined by the nonspiking dynamics and the value of the somatic voltage threshold ($V_{th} = 1$), it is independent of the spike amplitude β and the spike duration T_a, as can be seen in Figures 6 (a) and (b). According to (4.1), I_{th} increases linearly with γ and G_L and increases monotonically with L such that $I_{th} \to G_L + \gamma$ as $L \to \infty$. These relationships are reflected in Figures 7 (a)–(c). A biophysical understanding of these relationships follows directly from the interpretation of $I_{th} = G_L + \gamma \tanh(L)$ as the nondimensional input conductance of the neuron at the soma, where G_L is the somatic membrane conductance and $\gamma \tanh(L)$ is the nondimensional input conductance of dendrite at the somatodendritic junction [18].

By nondimensionalizing the system, we have lost explicit dependence of the threshold current I_{th} on several biophysical parameters including the leakage reversal potential of the dendrite E_{LD}. The relationships between I_{th} and dendritic parameters γ and L that were described above assume that the dendrite acts as a hyperpolarizing "load" on the soma; i.e., it assumes that $E_{LD} < V_{th}$. By inspecting the dimensional form of I_{th}

$$\overline{I}_{th} = g_L(V_{th} - E_L) + \gamma g_{LD}(V_{th} - E_{LD}) \tanh(\ell/\lambda), \tag{4.3}$$

we can clearly see that, when $E_{LD} < V_{th}$, the threshold current $\overline{I}_{th}$ increases with increasing γ and $L = \frac{\ell}{\lambda}$, but when $E_{LD} > V_{th}$, the threshold current $\overline{I}_{th}$ decreases with increasing γ and L. This agrees with the physical intuition of the load properties of dendrites. (Note, however, that this "intuitive" relationship does not hold for all neuronal models; see [36].)

The dashed lines in Figures 6 and 7 represent the value of the applied current above which periodic oscillations can be sustained via the ping-pong effect. Note that, for all parameters $(\beta, T_a, \gamma, L, G_L)$, there exists a critical value below which ping-pong oscillations do not exist.

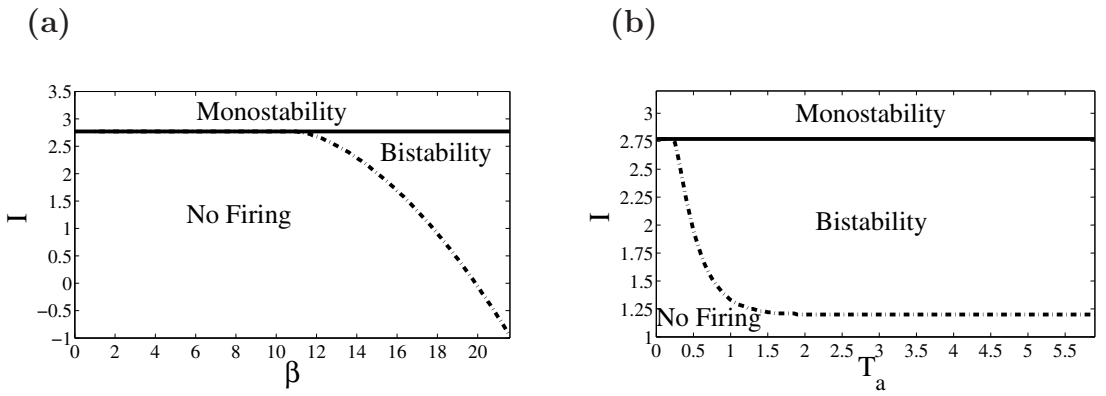

Figure 6. Effects of altering spike parameters on the size of the bistable region using the sigmoidal spike. *In this figure and all subsequent figures, the solid line represents I_{th} (i.e., the curve in parameter space above which the quiescent solution does not exist), and the dash-dotted line represents the minimum amount of applied current needed to sustain oscillations via the ping-pong effect (i.e., the curve in parameter space where the stable oscillatory solution first coexists with the stable quiescent solution). Thus, the spikes that occur in regions labeled "Bistability" arise for a different reason than spikes that occur in the regions labeled "Monostability."* (a) *Two parameter bifurcation diagram for the current applied to the soma I versus spike amplitude β. Parameters are $T_a = 0.2$, $V_R = -2$, $\gamma = 1$, $L = 1$, and $G_L = 2$.* (b) *I versus spike duration T_a bifurcation diagram. Parameters are $\beta = 10$, $V_R = -2$, $\gamma = 1$, $L = 1$, and $G_L = 2$.*

For sufficiently low values of any of the parameters, somatic dynamics dominate the behavior of the system. Thus, the somatic potential cannot overshoot its steady-state value, and ping-pong oscillation cannot occur.

Figure 6 (a) shows that a sufficiently large spike amplitude β is needed in order for ping-pong induced oscillations to occur and bistability to exist. Furthermore, as β is increased, ping-pong induced oscillations can occur at lower levels of the somatic applied current, and the size of the bistable region is increased. Thus, larger somatic spikes promote ping-pong oscillations. A large spike amplitude causes greater depolarization of the proximal dendrite after a spike and therefore increases the postspike depolarizing current flowing from the dendrite into the soma. This in turn helps the somatic potential to overshoot the quiescent steady-state, which leads to ping-pong oscillations.

Figure 6 (b) shows that, as the duration of the spike T_a increases, there is a decrease in the level of the applied current at which the onset of ping-pong oscillations occurs, and therefore there is an increase in the size of the bistable region. However, as T_a increases, the applied current above which ping-pong oscillations can occur approaches a minimal value. This minimal value can be explained as follows. When T_a is large, the somatic potential is held at a depolarized value near β for a long time, allowing the dendritic potential to nearly equilibrate with the somatic potential. Therefore, further increases in T_a will result in only insignificant increases in the proximal dendritic potential and thus do not further significantly promote the ping-pong effect.

Figure 7 (a) shows the two parameter bifurcation diagram of the applied current versus the parameter γ, (2.9). For the ping-pong effect to occur, γ must be above a critical value. Increasing γ beyond this critical value decreases the amount of applied current needed to

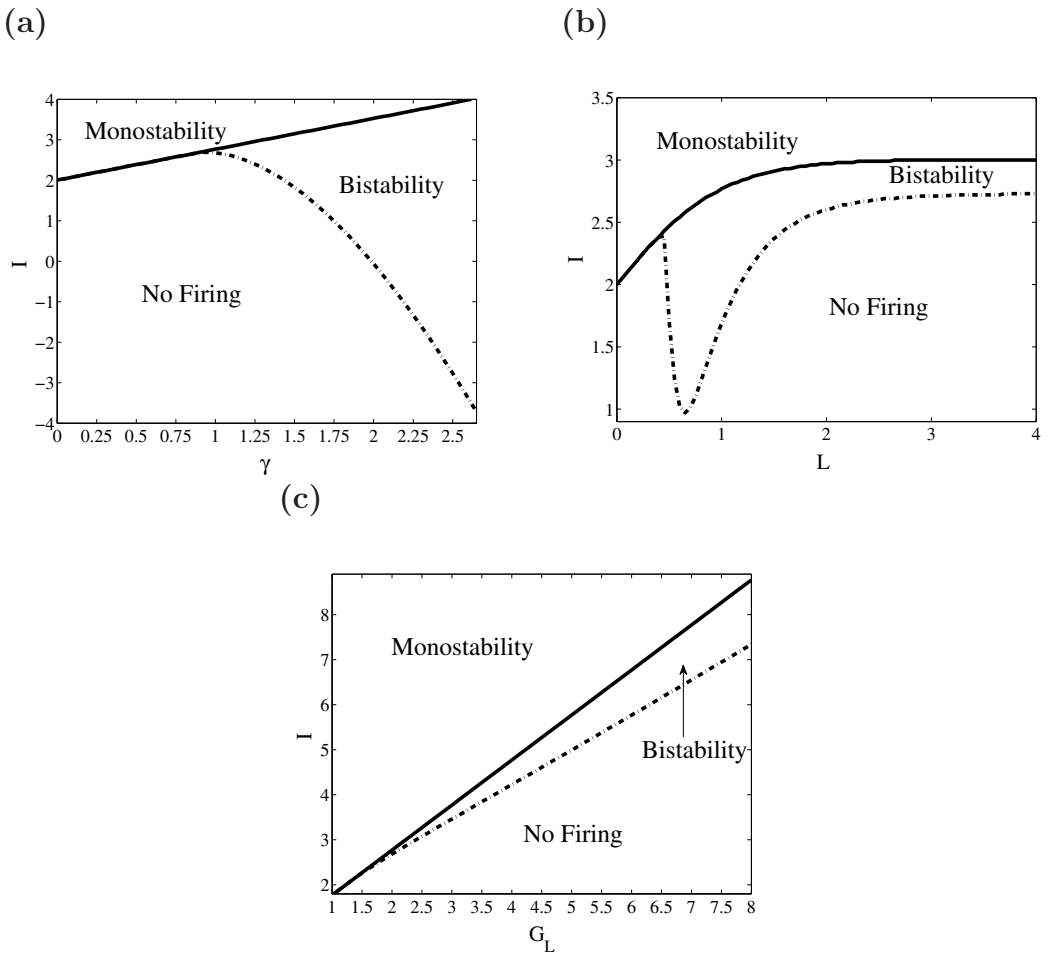

Figure 7. Effects of altering passive neuron parameters on the size of the bistable region using the sigmoidal spike. (a) *Two parameter bifurcation diagram of the applied current versus the parameter γ, which scales the influence of the dendrite on the soma. Parameters are $\beta = 12$, $T_a = 0.2$, $V_R = -2$, $L = 1$, and $G_L = 2$.* (b) *Two parameter bifurcation diagram of the applied current versus the electrotonic length of the dendrite, L. Parameters are $\beta = 16$, $T_a = 0.2$, $V_R = -2$, $\gamma = 1$, and $G_L = 2$.* (c) *Two parameter bifurcation diagram of the applied current I versus the nondimensional somatic leakage conductance, G_L. Parameters are $\beta = 12$, $T_a = 0.2$, $V_R = -2$, $\gamma = 1$, and $L = 1$.*

sustain the ping-pong effect. Note that γ scales the somatodendritic current (i.e., $\gamma \frac{\partial V}{\partial x}(0,t)$). For small γ, the somatodendritic current is small and has an insignificant effect on somatic dynamics; thus ping-pong oscillations cannot occur. As γ increases, the strength of the depolarizing current that flows from the dendrite into the soma after the spike increases, and therefore ping-pong oscillations are promoted.

Figure 7 (b) plots the two parameter bifurcation diagram of the applied current versus the electrotonic length of the dendrite L. Similar to its dependence on γ, ping-pong oscillations can occur only above a critical value of L, and the applied current needed to sustain ping-pong oscillations decreases with increasing L. However, in contrast to the dependence on γ, there is

an optimal value of L that produces the lowest level of applied current above which ping-pong oscillations can be sustained. This behavior arises from the spatial properties of the dendrite. At sufficiently large L, the proximal portion of the dendrite becomes significantly more depolarized than the distal portion during the somatic spike. Therefore, immediately after the spike, current flowing from the depolarized proximal dendrite must be divided between the soma and the distal portion as opposed to simply flowing into the soma. Thus, increasing L beyond a critical value deters ping-pong oscillations. Note that, for similar reasons, there will be an optimal dendritic diameter for promoting ping-pong activity. These results are related to the results on the optimal dendrite diameter for signal transmission by Holmes [15] and Nadim and Golowasch [27].

Figure 7 (c) plots the two parameter bifurcation diagram of the applied current versus the nondimensionalized somatic leakage conductance G_L, (2.10). The figure shows that, if the soma is too leaky, the ping-pong effect cannot occur. Above a critical somatic leakiness, ping-pong oscillations can occur, but a greater amount of current is needed to drive the oscillations as G_L increases. On the other hand, the size of the region of bistability increases as G_L is increased. When G_L is increased, relatively more current is drawn into the soma from the dendrite after the somatic spike; this acts to facilitate the onset of ping-pong oscillations. However, there is also an overall increase in the somatic input conductance with increased G_L; thus more current is required to depolarize the soma to threshold and induce oscillations.

4.3. The linear spike. The sigmoidal spike considered in the previous section had an abrupt repolarization. Here, we explicitly examine the effect of the rate of repolarization on firing dynamics by considering a spike with a linear repolarization. When the voltage at the soma reaches threshold, the "linear" spike instantaneously increases the somatic voltage to a value β and then linearly decreases the somatic voltage at a constant rate $\frac{V_R-\beta}{T_a}$ until it reaches V_R (see Figure 8 (a)). The functional form of the linear spike is

$$h(t) = \left(\frac{V_R - \beta}{T_a}\right) t + \beta, \quad t \in (0, T_a]. \tag{4.4}$$

Once again, β represents the maximum somatic potential during the spike, T_a is the duration of the spike, and V_R is the value of the somatic potential at the end of the spike.

As in the case of the sigmoidal spike, bistability between periodic firing and quiescence can occur in the model with the linear spike as a result of a somatodendritic ping-pong effect. In fact, the dependence on parameters as shown by the two parameter bifurcation diagrams for the linear spike are qualitatively similar to those for the sigmoidal spike except for the diagrams involving the duration of the spike T_a. Compare the diagram for I versus T_a in Figure 8 (b) to that of Figure 6 (b). Although the transition to bistability occurs similarly for both spike types, bistability eventually disappears as T_a becomes too large for the case of the linear spike. This results from the decrease in the rate of repolarization of the linear spike as its duration becomes larger. For sufficiently large values of T_a, the proximal dendritic potential is able to closely track the somatic potential during the spike as it decreases to the reset potential V_R. Thus, at the end of the spike, there is no longer a large gradient in the membrane potential between the proximal dendrite and the soma, and the ping-pong effect ceases to occur.

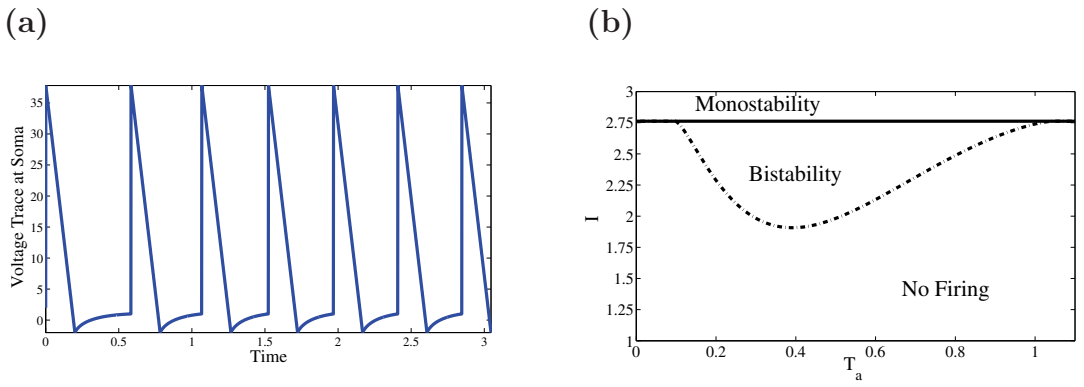

Figure 8. Ball-and-stick model behavior with the linear spike function. (a) *Voltage trace at the soma ($x = 0$) with the linear spike function (4.4). After reaching threshold, the somatic potential abruptly increases to a value β and then linearly decreases to V_R. Parameters are $\beta = 38$, $T_a = 0.2$, $V_R = -2$, $I = 2$, $\gamma = 1$, $L = 1$, and $G_L = 2$.* (b) *Effects of altering spike duration on the size of the bistable region using the linear spike. Parameters are $\beta = 30$, $V_R = -2$, $\gamma = 1$, $L = 1$, and $G_L = 2$.*

5. Two-compartment LIF model. A standard simplification of the ball-and-stick model is to lump the passive dendritic cable into a single passive compartment that is electrically coupled to the soma [2, 9, 23, 28]. This simplification often leads to greater mathematical tractability while still capturing the essential dynamics of the neuronal model. Here we consider a two-compartment model in which the somatic dynamics are described by the LIF model that explicitly includes a spike and the dendrite is modeled as a single passive compartment. In this case, we are able to reduce the dynamics of the system to consideration of a one-dimensional map (for a similar approach, see [3]). We then show that the dynamics of the full ball-and-stick model are well captured by the simpler two-compartment model.

The dendrite is now modeled as a single passive compartment that is electrically coupled to the soma

$$C_m \frac{d\overline{V}_D}{d\bar{t}} = -g_{LD}(\overline{V}_D - E_{LD}) + \frac{g_c}{A_D}(\overline{V}_S - \overline{V}_D), \tag{5.1}$$

where $\overline{V}_D$ and $\overline{V}_S$ are the membrane potentials of the dendritic and somatic compartments, respectively, C_m is the membrane capacitance, g_{LD} is the dendritic leakage conductance, E_{LD} is the dendritic leakage reversal potential, g_c is the somatodendritic coupling conductance, and A_D is the area of the dendritic compartment.

The soma is modeled as an LIF compartment. The dynamics for the nonspiking portion of the somatic membrane potential are governed by

$$C_m \frac{d\overline{V}_S}{d\bar{t}} = -g_{LS}(\overline{V}_S - E_{LS}) + \frac{g_c}{A_S}(\overline{V}_D - \overline{V}_S) + \overline{I}, \tag{5.2}$$

where E_{LS} is the leakage reversal potential of the somatic compartments, g_{LS} is the somatic leakage conductance, $\overline{I}$ is the applied current to the soma, and A_S is the area of the somatic compartment. As in the previous section, when $\overline{V}_S$ reaches a threshold voltage at time $\bar{t}_s^j$

($\overline{V}_S(\overline{t}_s^j) = \overline{V}_{th}$), the jth spike is elicited in the soma. The transmembrane potential of the soma during the spike is given by

$$\overline{V}_S(\overline{t}) = \overline{h}(\overline{t} - \overline{t}_s^j), \quad \overline{t} \in (\overline{t}_s^j, \overline{t}_s^j + \overline{T}_a], \tag{5.3}$$

where $\overline{h}(\overline{t})$ is a function that describes the shape of the spike. After a time $\overline{T}_a$, the somatic dynamics are switched back to (5.2) at $\overline{t} = \overline{t}_s^j + \overline{T}_a$.

In nondimensional form, the LIF two-compartment model is given by

$$\frac{dV_D}{dt} = -V_D + \alpha g(V_S - V_D), \tag{5.4}$$

$$\begin{cases} \dfrac{dV_S}{dt} = -g_{lk}V_S + g(V_D - V_S) + I & \text{if } t \notin (t_s, t_s^j + T_a], \\ V_S(t) = h(t - t_s^j) & \text{if } t \in (t_s^j, t_s^j + T_a], \end{cases} \tag{5.5}$$

where $V_n(t) = \frac{\overline{V}_n(\overline{t}/\tau_D) - E_{LD}}{\overline{V}_{th} - E_{LD}}$ and $n = S, D$, $\tau_D = C_m/g_{LD}$, $\alpha = \frac{A_S}{A_D}$, $g = \frac{g_c}{A_S g_{LD}}$, $g_{lk} = g_{LS}/g_{LD}$, $I = \frac{\overline{I} + g_{LS}(E_{LS} - E_{LD})}{g_{LD}(\overline{V}_{th} - E_{LD})}$, $V_{th} = \frac{\overline{V}_{th} - E_{LD}}{\overline{V}_{th} - E_{LD}} = 1$, $h(t) = \frac{\overline{h}(\overline{t}/\tau_D) - E_{LD}}{\overline{V}_{th} - E_{LD}}$, and $t = \frac{\overline{t}}{\tau_D}$.

An analysis of the nonspiking portion of system (5.4)–(5.5) shows that the two-compartment model has a unique quiescent steady-state (V_D^{ss}, V_S^{ss}) given by

$$V_D^{ss} = \frac{I\alpha g}{g + g_{lk}(1 + g\alpha)}, \tag{5.6}$$

$$V_S^{ss} = \frac{I(1 + \alpha g)}{g + g_{lk}(1 + g\alpha)}. \tag{5.7}$$

This steady-state is always stable for biophysically realistic parameters, but it exists only when $V_S^{ss} < 1$, which is the case when the current applied to the soma is less than a threshold value I_{th}

$$I_{th} = g_{lk} + \frac{g}{1 + \alpha g}. \tag{5.8}$$

If $I > I_{th}$, then $V_S^{ss} > 1$, which implies that the steady-state does not exist and the neuron will undergo repetitive firing. As with the ball-and-stick model, the threshold current I_{th} is equal to the nondimensional input conductance and separates the influences of the LIF soma (g_{lk}) and those of the dendrite ($\frac{g}{1+\alpha g}$). Note that, as the coupling conductance $g \to 0$ or the relative size of the soma compared to the dendrite $\alpha \to \infty$, then I_{th} approaches the value that would be obtained for the standard LIF model.

6. One-dimensional map for the two-compartment model. In this section, we derive a one-dimensional return map that takes the state of the neuron at the end of the jth spike to the state of the neuron at the end of the $j + 1$st spike or to the quiescent steady-state. This one-dimensional map completely captures the firing dynamics of the two-compartment model.

Assume that the neuron model is at the end of the jth spike, i.e., $t = t_s^j + T_a$, and that the somatic voltage is at the reset potential V_R and the dendritic voltage is at some potential V_D^j,

$$\begin{pmatrix} V_D(t_s^j + T_a) \\ V_S(t_s^j + T_a) \end{pmatrix} = \begin{pmatrix} V_D^j \\ V_R \end{pmatrix}.$$

Until the next spike is elicited ($t \in (t_s^j + T_a, t_s^{j+1})$), the dynamics of the neuron are given by the solution for the nonspiking portion of the system

$$\begin{pmatrix} V_D(t) \\ V_S(t) \end{pmatrix} = c_1(V_D^j)\, e^{\lambda_1(t-(t_s^j+T_a))}\, \overrightarrow{u_1} + c_2(V_D^j)\, e^{\lambda_2(t-(t_s^j+T_a))}\, \overrightarrow{u_2} + \begin{pmatrix} V_D^{ss} \\ V_S^{ss} \end{pmatrix}, \tag{6.1}$$

where

$$\lambda_1 = \frac{1}{2}\left(-(1+g+g_{lk}+g\alpha) - \sqrt{(1+g+g_{lk}+g\alpha)^2 - 4(g+g_{lk}+g\alpha g_{lk})}\right),$$
$$\lambda_2 = \frac{1}{2}\left(-(1+g+g_{lk}+g\alpha) + \sqrt{(1+g+g_{lk}+g\alpha)^2 - 4(g+g_{lk}+g\alpha g_{lk})}\right),$$
$$\overrightarrow{u_1} = \begin{bmatrix} 1 \\ \frac{1+g\alpha+\lambda_1}{g\alpha} \end{bmatrix}, \quad \overrightarrow{u_2} = \begin{bmatrix} 1 \\ \frac{1+g\alpha+\lambda_2}{g\alpha} \end{bmatrix}$$

are the eigenvalues and eigenvectors of the system and

$$\begin{pmatrix} c_1(V_D^j) \\ c_2(V_D^j) \end{pmatrix} = \left[\overrightarrow{u_1}\ \overrightarrow{u_2}\right]^{-1} \begin{pmatrix} V_D^j - V_D^{ss} \\ V_R - V_S^{ss} \end{pmatrix}$$

are integration constants that depend on V_D^j.

Whether or not the neuron reaches threshold and fires the $j+1$st spike depends on the parameter values and the dendritic voltage at the end of the jth spike, V_D^j. If parameters are such that $I > I_{th}$, the somatic voltage will always reach threshold and a spike will be elicited. However, even if the steady-state somatic potential is below threshold ($V_S^{ss} < V_{th} = 1$), the somatic voltage can reach threshold and the cell can fire a spike via the somatodendritic ping-pong effect, but only if V_D^j is above a critical voltage V_D^*.

The time of the $j+1$st spike and the corresponding interspike interval $\Delta t_s^j = t_s^{j+1} - t_s^j$ are found by setting the somatic voltage to the threshold potential ($V_S(t_s^{j+1}) = V_{th} = 1$) and finding the smallest positive solution of the resulting transcendental equation for Δt_s^j

$$1 = c_1(V_D^j)\, e^{\lambda_1(\Delta t_s^j - T_a)}\, \frac{1+g\alpha+\lambda_1}{g\alpha} \;+\; c_2(V_D^j)\, e^{\lambda_2(\Delta t_s^j - T_a)}\, \frac{1+g\alpha+\lambda_2}{g\alpha} \;+\; V_S^{ss}.$$

If a positive solution to the above equation does not exist, the neuron evolves to the quiescent steady-state without firing.

To determine the critical voltage V_D^*, we first examine the V_S, V_D phase plane as illustrated in Figure 9. Note that the trajectory starting at (V_D^*, V_R) separates phase space into two regions. For $V_D < V_D^*$, trajectories that start at (V_D, V_R) evolve to the steady-state (V_D^{ss}, V_S^{ss}) without crossing threshold $V_S = 1$, indicating that the cell does not spike again. For $V_D > V_D^*$, trajectories that start at (V_D, V_R) eventually cross threshold $V_S = 1$, indicating that the cell spikes, i.e., V_S overshoots V_S^{ss} and $V_{th} = 1$. The trajectory starting at (V_D^*, V_R) hits the threshold $V_S = 1$ but does not cross it. This implies that this critical trajectory hits $V_S = 1$ at the point where it crosses the V_S-nullcline, i.e., at $(V_D, V_S) = \left(\frac{g_{lk}+g-I}{g}, 1\right)$. Plugging this information into the solution for the nonspiking portion of the system (6.1), we obtain a

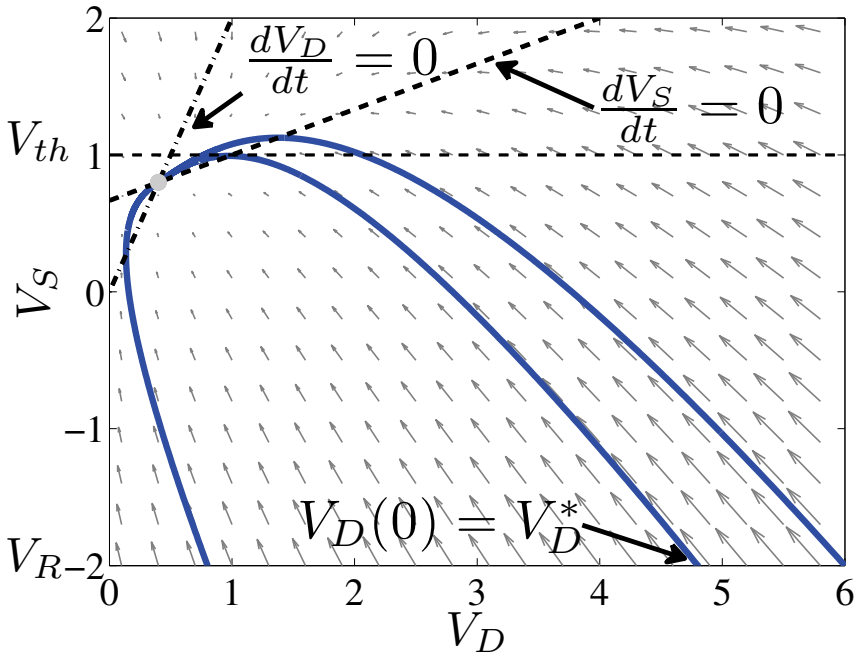

Figure 9. Phase plane for the nonspiking portion of the two-compartment model. *The thin dashed line is* $V_S = 1$, *the thicker dashed line is* $\frac{dV_S}{dt} = 0$, *the thick dash-dotted line is* $\frac{dV_D}{dt} = 0$, *and the steady-state is plotted as the grey dot at the intersection of the two nullclines. The trajectory that begins at* (V_D^*, V_R) *touches the somatic threshold value of* 1 *but does not cross it. This trajectory separates trajectories that cross threshold* $V_{th} = 1$ *and those that directly converge to the steady state without crossing threshold. Note that, once the trajectory crosses threshold, the dynamics are then governed by the spiking portion of the model after which the somatic potential is brought back to* $V_R = -2$.

system of two transcendental equations

$$\begin{bmatrix} \frac{g_{lk}+g-I}{g} \\ 1 \end{bmatrix} = c_1(V_D^*)\ e^{\lambda_1 t^*}\ \overrightarrow{u_1}\ +\ c_2(V_D^*)\ e^{\lambda_2 t^*}\ \overrightarrow{u_2}$$

that can be used to solve for the two unknowns V_D^* and t^*, where t^* is the time it takes for the trajectory to flow from the point (V_D^*, V_R) to the point $\left(\frac{g_{lk}+g-I}{g}, 1\right)$.

If the neuron fires a $j+1$st spike, the dendritic voltage at the onset of the spike is

$$V_D(t_s^{j+1}) = \phi_1(V_D^j) := c_1(V_D^j)\ e^{\lambda_1(\Delta t_s^j - T_a)}\ +\ c_2(V_D^j)\ e^{\lambda_2(\Delta t_s^j - T_a)}\ +\ V_D^{ss}. \tag{6.2}$$

The dendritic voltage at the end of the spike is obtained by solving (5.4) from time $t = t_s^{j+1}$ to $t = t_s^{j+1} + T_a$ using $V_D(t_s^{j+1})$ as the initial condition and the prescribed shape of the somatic potential during the spike, (5.5),

$$V_D(t_s^{j+1} + T_a) = \phi_2(V_D^j) := e^{-(1+\alpha g)T_a}\left(V_D(t_s^{j+1}) + \alpha g \int_0^{T_a} h(s) e^{(1+\alpha g)s} ds\right). \tag{6.3}$$

By convolving the maps for the subthreshold dynamics, (6.2), and the spike dynamics, (6.3), we can define a map that takes the state of the neuron at the end of the jth spike (V_D^j, V_R) to the state of the neuron at the end of the $j+1$st spike (V_D^{j+1}, V_R) or the steady-state (V_D^{ss}, V_S^{ss})

(6.4)
$$V_D^{j+1} = \phi_2 \circ \phi_1(V_D^j) = \begin{cases} e^{-(1+\alpha g)T_a}\Big(c_1(V_D^j)e^{\lambda_1(\Delta t_s^j - T_a)} \\ \qquad + c_2(V_D^j)e^{\lambda_2(\Delta t_s^j - T_a)} + V_D^{ss} + \alpha g \int_0^{T_a} h(s)e^{(1+\alpha g)s}ds\Big) & \text{if } V_D^j > V_D^*, \\ V_D^{ss} & \text{if } V_D^j \le V_D^*. \end{cases}$$

Note that, when $V_D^j > V_D^*$, the spike map ϕ_2 is linear, and, in the limit as $T_a \to 0$ and $h(t) \to \beta\delta(t)$, ϕ_2 simply increases V_D by a constant $\beta\alpha g$ [22]. Note also that fixed points of the above map with $V_D^j = V_D^{ss}$ correspond to the quiescent state in the full system, whereas fixed points with $V_D^j > V_D^{ss}$ correspond to periodic firing in the full system.

7. Two-compartment model behavior.

We now examine the behavior of the two-compartment model with two different spike functions: a square spike and a linear spike. As with the ball-and-stick model, we find that the two-compartment model exhibits bistable behavior arising from the somatodendritic ping-pong effect and displays very similar dependence on parameters.

7.1. Square spike.

We describe the spike by a square pulse

$$h(t) = \begin{cases} \beta & \text{if } 0 < t < T_a, \\ V_R & \text{if } t = T_a. \end{cases} \tag{7.1}$$

The parameter β represents the maximal somatic potential that is reached during the spike, T_a is the duration of the spike, and V_R is the value of the somatic potential after the spike has completed. Note that the square pulse is the limit of the sigmoidal spike function (4.2) as $p \to \infty$.

Figure 10 (a) plots an example of the somatic and dendritic membrane potentials found using square spikes with $I = 2.5 < I_{th} = 2.6$. Recall that if $I > I_{th}$, the quiescent steady-state does not exist, and the system is guaranteed to be in the oscillatory regime. However, as was the case for the ball-and-stick model, stable periodic firing can coexist with the quiescent steady-state in the two-compartment model for $I < I_{th}$. The return map (6.4) corresponding to the system simulated in Figure 10 (a) is plotted in Figure 10 (b). Note that the map has two stable fixed points: The lower fixed point corresponds to a stable quiescent state in the two-compartment model, and the upper fixed point corresponds to stable periodic firing. Below, we use the return map to determine the regions of parameter space in which a stable quiescent state exists and stable periodic firing exists in the two-compartment model neuron.

Altering parameters in the two-compartment model with the square spike yields very similar dynamics to those of the ball-and-stick model with the sigmoidal spike. This is clearly

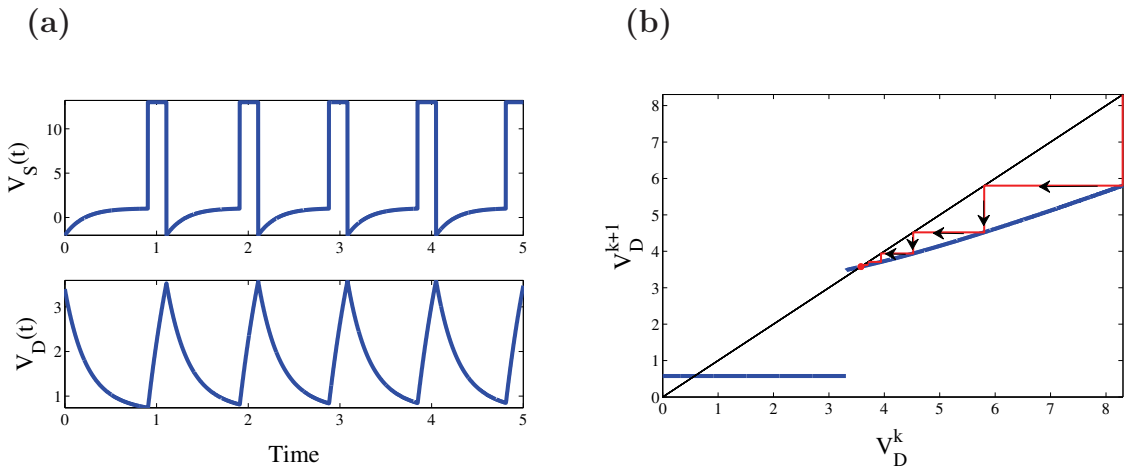

Figure 10. The ping-pong effect and bistability in the two-compartment model with the square spike. (a) *Voltage traces of the somatic and dendritic compartments with the square spike as in* (7.1). *For the parameter values used,* $I < I_{th} = 2.6$, *and the ping-pong effect between the somatic and dendritic compartment potentials holds the system in the oscillatory regime.* (b) *The grey line plots the return map* (6.4) *derived from the two-compartment model with the square spike. The black line is identity line* $V_D^{k+1} = V_D^k$. *The map has two stable fixed points indicating that the full two-compartment model displays bistability between periodic firing and the quiescent steady state: The lower fixed point corresponds the quiescent steady state* (V_D^{ss}, V_S^{ss}), *and the upper fixed point corresponds to periodic firing. Parameters for both plots are* $\beta = 13$, $T_a = 0.2$, $V_R = -2$, $g = 1.5$, $g_{lk} = 2$, $\alpha = 1$, *and* $I = 2.5$.

seen for spike amplitude β and spike duration duration T_a by comparing Figure 11 with Figure 6. The similarities are also seen for the passive membrane parameters by comparing Figures 12 and 7. The physical interpretation of the parameters g and g_{lk} in the two-compartment model corresponds well to the parameters γ and G_L in the ball-and-stick model. This correspondence is seen in the similarities of Figure 12 (a) and (c) and Figure 7 (a) and (c). The ratio of the somatic-to-dendritic surface areas α in the two-compartment model loosely corresponds to the inverse of the length of the dendrite $1/L$ in the ball-and-stick model, as reflected in the similarities between Figure 12 (b) and Figure 7 (b). It is important to note that all of the biophysical mechanisms underlying the two parameter bifurcation diagrams described in section 4 for the ball-and-stick model carry over to the two-compartment model.

7.2. Linear spike. The linear spike is described in (4.4) of section 4.3. Figure 13 (a) plots an example of the somatic and dendritic voltage traces found using the linear spike. Somatodendritic ping-pong causes the system to display oscillatory behavior even when the applied current to the soma is below I_{th}.

As was the case for the ball-and-stick model, the two parameter bifurcation diagrams for the two-compartment model with the linear spike and the square spike are qualitatively the same except for the diagram plotting applied current I versus the spike duration T_a (Figure 13 (b)). Moreover, Figure 13 (b) shows that altering the duration of the linear spike yields qualitatively similar dynamics to those of the ball-and-stick model with the linear spike.

Thus, we have demonstrated that the two-compartment model captures the qualitative

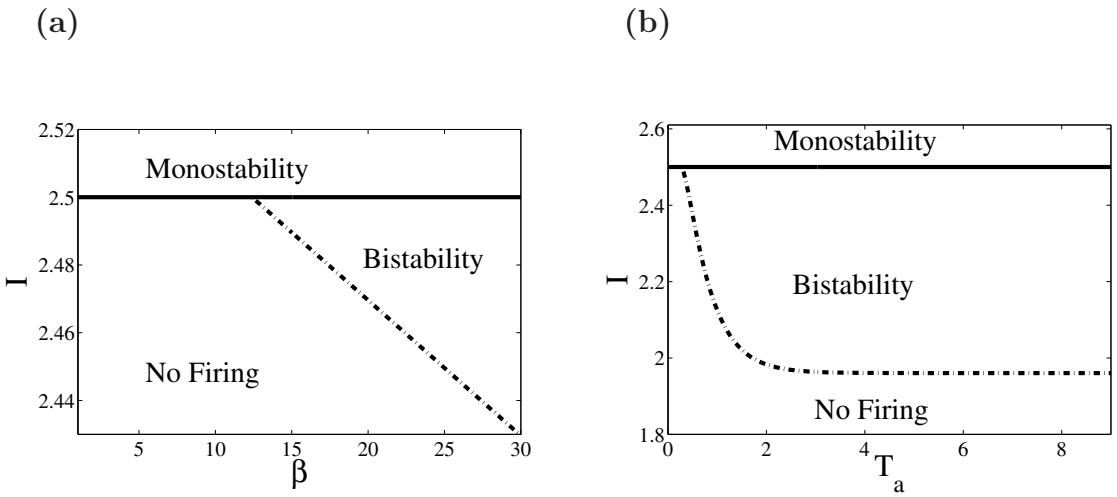

Figure 11. Effects of changing spike parameters in the two-compartment model with the square spike. (a) *Two parameter bifurcation diagram of applied current I versus the maximum somatic depolarization during the spike, β. Parameters are $T_a = 0.2$, $V_R = -2$, $g = 1$, $g_{lk} = 2$, and $\alpha = 1$.* (b) *Two parameter bifurcation diagram of applied current versus the duration of the spike, T_a. Both diagrams are qualitatively similar to the corresponding diagrams generated for the ball-and-stick model with the sigmoidal spike (Figure 6). Parameters are $\beta = 10$, $V_R = -2$, $g = 1$, $g_{lk} = 2$, and $\alpha = 1$.*

behavior of the ball-and-stick model when considering dependence of the firing dynamics on parameters.

8. Discussion. In this article, we examine the effects of a passive dendrite on the firing dynamics of an LIF neuron that explicitly includes a spike. We model the dendrite as either a passive cable using the cable equation (a ball-and-stick model) or as a single passive compartment (a two-compartment model). For each model, we are able to derive the analytical solution and reduce the system dynamics down to consideration of a return map. Using the map, we find that dendritic properties can significantly change the firing dynamics of the system. Under certain conditions, the addition of the dendrite can change the LIF model from type 1 excitability to type 2 excitability and induce bistability between periodic firing and the quiescent state. We identify the mechanism that causes the periodic behavior in the bistable regime as somatodendritic ping-pong. Furthermore, we use the return map to fully explore the model parameter space in order to find regions where this bistable behavior occurs. We then give physical interpretations for the dependence of the bistable behavior on model parameters. Finally, we demonstrate that the simpler two-compartment model displays qualitatively similar dynamics to those of the more complicated ball-and-stick model. Furthermore, the appendix shows that the analysis we present here can be extended to include dendritic point source inputs. However, we find that the addition of these inputs does not change the qualitative dynamics presented in the main paper.

Previous work has examined the effects of dendritic properties on the frequency-input (f-I) relationship of neuronal oscillators [3, 21, 24, 36, 38]. In two closely related studies, Lánský and Rodriguez [21] and Bressloff [3] examined how the addition of a passive dendritic

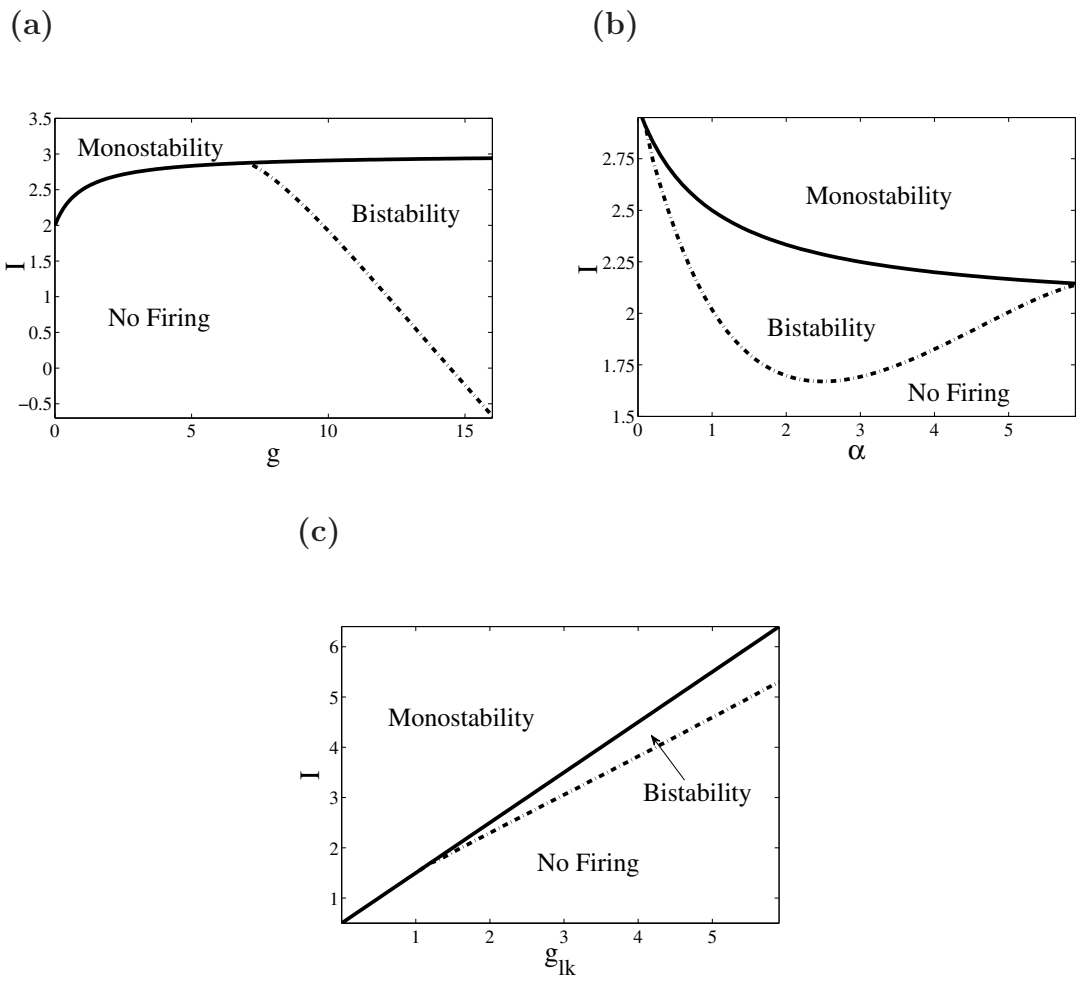

Figure 12. Effects of altering passive membrane parameters in the two-compartment model with the square spike. (a) *Two parameter bifurcation diagram for applied current I versus coupling conductance g. Parameters are $\beta = 5$, $T_a = 0.2$, $V_R = -2$, $g_{lk} = 2$, and $\alpha = 1$.* (b) *Two parameter bifurcation diagram for applied current I versus soma to dendrite membrane area α. Parameters are $\beta = 25$, $T_a = 0.2$, $V_R = -2$, $g_{lk} = 2$, and $g = 1$.* (c) *Two parameter bifurcation diagram for applied current I versus somatic leakage conductance g_{lk}. Parameters are $\beta = 5$, $T_a = 0.2$, $V_R = -2$, $g = 1$, and $\alpha = 1$. Note the similarities between these diagrams and corresponding diagrams generated for the ball-and-stick model with the sigmoidal spike in Figure 7.*

compartment can affect the firing dynamics of the LIF neuron. These studies found that the addition of the dendrite delays the onset of oscillations as input to the soma is increased and decreases the firing frequency at any given input level. These results are to be expected when one interprets the dendritic compartment as a passive load on the soma (see, however, [36]). Here, we show that, in addition to these effects, dendrites can induce bistability between periodic firing and quiescence. The previous studies did not observe this bistable behavior because they did not include the effects of the somatic spike on the dendritic compartment.

We have identified the mechanism for periodic firing in the bistable regime as somato-

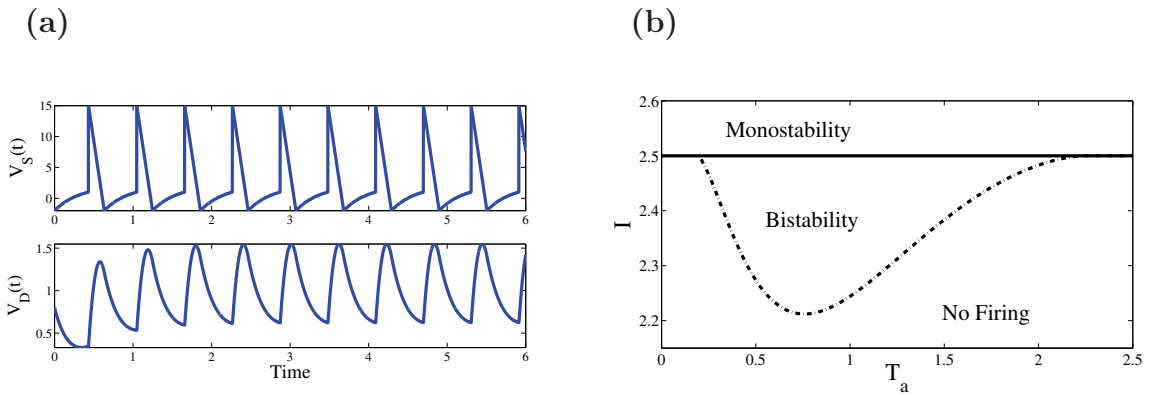

Figure 13. Two-compartment model behavior with the linear spike function. (a) *Voltage traces of the somatic and dendritic compartments with the linear spike function. Parameters are* $\beta = 15$, $T_a = 0.2$, $V_R = -2$, $g = 1$, $g_{lk} = 2$, $I = 6$, *and* $\alpha = 1$. (b) *Two parameter bifurcation diagram of applied current* I *versus* T_a. *Note that this diagram is qualitatively similar to the corresponding diagram for the ball-and-stick model with the linear spike (Figure 8 (b)). Parameters are* $\beta = 30$, $V_R = -2$, $g = 1$, $g_{lk} = 2$, *and* $\alpha = 1$.

dendritic ping-pong [2, 39]. Somatodendritic ping-pong has been previously described in the context of neuronal bursting dynamics [2, 9, 20, 28, 39]. Bose and Booth [2] showed that in order for somatodendritic ping-pong bursting activity to occur in two-compartment models, the coupling conductance between the somatic and dendritic compartments and the integration time constant of the dendritic compartment must be tightly tuned so as to allow the dendritic compartment time to be sufficiently depolarized after a somatic spike. The relative simplicity of our LIF models enables us to expand on these requirements by explicitly examining how the spike properties and dendritic cable properties affect neuronal firing. For example, we find that both the size (amplitude and duration) of the somatic spike as well as the rate of repolarization of the soma must be sufficiently large in order for ping-ponging to occur. Furthermore, increasing the length of the dendrite generally promotes the ping-pong effect up to an optimal length. Increasing the dendritic reversal potential E_{LD} can promote the ping-pong effect as well. Note that adding active currents, e.g., a persistent sodium current, to the dendrite in our system would make it easier for the ping-pong effect to occur.

We have shown that the addition of a dendrite can fundamentally change the *f-I* curve of the LIF model. In the standard LIF model, oscillations can occur at arbitrarily low frequencies and increase rapidly with increasing input. This *f-I* relationship is characteristic of Hodgkin's type 1 neural excitability [14]. Intuitively, if a dendritic load is added to the standard LIF model, one would expect a rightward shift in the *f-I* curve while retaining the type 1 neural excitability [3, 21]. However, we find that when a spike is explicitly included in the LIF model, the addition of the dendrite can cause the onset of oscillations to arise at a nonzero frequency that is relatively insensitive to increases in input current. This relationship is characteristic of Hodgkin's type 2 neural excitability. The two types of neural excitability are known to be associated with particular bifurcations. Type 1 neural excitability is associated with the onset of oscillations arising from an infinite period bifurcation (saddle-node-on-an-invariant-cycle

(SNIC) bifurcation), and type 2 neural excitability is associated with the onset of oscillations arising from a Hopf bifurcation [16]. This would imply that oscillations in the standard LIF model arise from a discontinuous bifurcation that is reminiscent of a SNIC bifurcation (see Figure 4 (a)). When the effects of the dendrite are sufficiently large and a somatic spike is explicitly included, the addition of the dendrite can cause oscillations in the LIF model to arise from a discontinuous bifurcation that is reminiscent of a subcritical Hopf bifurcation (Figure 4 (b)). Thus, the transition between the two types of bifurcations would appear to involve the discontinuous equivalent of a Takens–Bogdanov bifurcation [16]. Future work must be done to fully expound the details of the corresponding bifurcation structure of the system and to show that these dynamics extend to continuous systems.

The influence of dendrites on transitions from type 1 to type 2 excitability, as well as the associated bifurcations and changes in *f-I* curves, is of importance to many areas of neuroscience. For example, (1) the encoding properties of a neuron are reflected in the shape of its *f-I* curve [5, 21]. Lánský and Rodriguez [21] showed that the addition of a dendritic compartment to the LIF neuron can increase its encoding range. However, we show that the addition of the dendrite can cause the LIF neuron to change from type 1 to type 2 excitability, which is typically associated with a smaller encoding range than type 1 neurons. (2) Type 2 excitability is often associated with a region of bistability which allows the neuron to behave like a neuronal switch; i.e., the neuron can change between periodic firing and quiescence in response to transient inputs. This type of behavior has been observed in parts of the central nervous system ranging from the spinal cord [30] to the neocortex [13] and is hypothesized to be closely related to short-term memory. (3) Type 2 neurons respond best to fluctuating inputs around a characteristic frequency, whereas type 1 neurons summate inputs across a broad range of frequencies. Types 1 and 2 neurons have therefore been labeled integrators and resonators, respectively [16, 29]. (4) The phase response curve (PRC) differs between types 1 and 2 neurons [35]; near the onset of oscillations, type 1 neurons display a monophasic PRC, whereas type 2 neurons can display biphasic PRCs. The different PRC shapes for the two types of excitability are known to have a critical influence on the synchronization properties of neuronal networks [12]. Therefore, a deeper understanding of the mechanisms by which the dendrite causes the transition from type 1 to type 2 excitability, and the associated changes in *f-I* curves, will be extremely valuable.

Appendix A. Dendritic inputs in the LIF ball-and-stick model. In this section, we discuss how point source inputs to the dendrite affect the dynamics we describe in the main paper. Specifically, by adding point source inputs to our model dendrite in (2.5)–(2.8) we arrive at

$$\frac{\partial V}{\partial t} = \frac{\partial^2 V}{\partial x^2} - V + I_d \delta(x - x_d), \tag{A.1}$$

$$\begin{cases} V(0,t) = h(t - t_s^j) & \text{if } t \in (t_s^j, t_s^j + T_a] \quad \text{[spike]}, \\ \dfrac{\partial V}{\partial t}(0,t) = -G_L V(0,t) + I + \gamma \dfrac{\partial V}{\partial x}(0,t) & \text{if } t \in (t_s^j + T_a, t_s^{j+1}] \quad \text{[nonspike]}, \end{cases} \tag{A.2}$$

$$\frac{\partial V}{\partial x}(L,t) = 0, \tag{A.3}$$

$$V(x, t_s^j) = V^j(x), \tag{A.4}$$

where I_d and x_d are, respectively, the strength and location of the point source input to the dendrite.

For the spike portion of the map, the addition of the dendritic point source input can be accounted for by adding the term $G^S(x, x_d)$ to (3.1),

$$V(x,t) = U(x,t) + h(t - t_s^j)\tilde{V}^{ss}(x) + G^S(x, x_d), \tag{A.5}$$

where

$$G^S(x, x_d) = \begin{cases} I_d \sinh(x)\cosh(L - x_d)/\cosh(L) & \text{if } 0 \le x \le x_d \le L, \\ I_d \sinh(x_d)\cosh(L - x)/\cosh(L) & \text{if } 0 \le x_d \le x \le L \end{cases} \tag{A.6}$$

is the Green's function for the system

$$\begin{aligned} &-\frac{d^2G^S}{dx^2} + G^S = I_d\delta(x - x_d), \\ &G^S(0) = 0, \\ &\frac{dG^S}{dx}(L) = 0. \end{aligned}$$

The solution of the spiking portion of the model (3.3) is then modified to be

$$\begin{aligned} V(x,t) = \sum_{m=0}^{\infty} \left(\tilde{V}_m^j + \tilde{V}_m^{ss} q_m(t - t_s^j) - \tilde{g}_m^S(x, x_d)\right) e^{-(1+\lambda_m^2)(t-t_s^j)} Y_m(x) \\ + h(t - t_s^j)\tilde{V}^{ss}(x) + G^S(x, x_d), \quad t \in [t_s^j, t_s^j + T_a), \end{aligned}$$

where

$$\tilde{g}_m^S(x, x_d) = \frac{\langle G^S(x, x_d), Y_m(x)\rangle}{\langle Y_m(x), Y_m(x)\rangle},$$

and the $Y_m(x)$ are given by (3.4). Thus, the membrane potential along the neuron at the end of the jth spike is

$$V^{j+\frac{1}{2}}(x) = V(x, t_s^j + T_a) = \sum_{m=0}^{\infty} \tilde{V}_m^{j+\frac{1}{2}} Y_m(x), \tag{A.7}$$

where

$$\tilde{V}_m^{j+\frac{1}{2}} = \left(\tilde{V}_m^j + q_m(T_a)\tilde{V}_m^{ss} - \tilde{g}_m^S(x, x_d)\right) e^{-(1+\lambda_m^2)T_a} + h(T_a)\tilde{V}_m^{ss} + \tilde{g}_m^S(x, x_d)$$

and the spike map (3.22) is now given by

$$\Phi_Y^S : \vec{V}^j \to \vec{V}^{j+\frac{1}{2}} = \Omega^S \vec{V}^j + (\Omega^S Q + H)\vec{V}^{ss} + (\mathbb{I} - \Omega^S)\vec{g}^S(x, x_d), \tag{A.8}$$

where Q, H, and Ω^S are given in (3.7)–(3.8).

For the nonspiking portion, we account for the point source dendritic input by changing (3.11) to

$$V_G^{ss}(x) = \rho\cosh(L-x) + G^{NS}(x,x_d), \tag{A.9}$$

where

$$G^{NS}(x,x_d) = \begin{cases} I_d a(x_d)\left[\frac{G_L}{\gamma}\sinh(x)+\cosh(x)\right] & \text{if } 0 \le x \le x_d \le L, \\ I_d b(x_d)\cosh(L-x) & \text{if } 0 \le x_d \le x \le L, \end{cases} \tag{A.10}$$

$$a(x_d) = \frac{\gamma\cosh(L-x_d)}{G_L\cosh(L)+\gamma\sinh(L)},$$

$$b(x_d) = \frac{G_L\sinh(x_d)+\gamma\cosh(x_d)}{\gamma\sinh(L)+G_L\cosh(L)}$$

is the Green's function for the system

$$-\frac{d^2G^{NS}}{dx^2} + G^{NS} = I_d\delta(x-x_d),$$

$$\frac{dG^{NS}}{dx}(0) = \frac{G_L}{\gamma}G^{NS}(0),$$

$$\frac{dG^{NS}}{dx}(L) = 0.$$

Thus, the map for the nonspiking portion is of the same form as in (3.20). The full map of the system can now be written as

$$\begin{aligned} \Phi_X &= \Phi_X^S \circ \Phi_X^{NS} : \overrightarrow{V}^{j+1} \\ &= \Omega^{NS,j} P\Omega^S R\ \overrightarrow{V}^j + \Omega^{NS,j}\left[P(\Omega^S Q + H)R - \mathbb{I}\right]\ \frac{\overrightarrow{V}^{ss}}{V^{ss}(0)} \\ &\quad + [P(\mathbb{I}-\Omega^S)R]\overrightarrow{g}^S(x,x_d) + \overrightarrow{V}_G^{ss}, \end{aligned} \tag{A.11}$$

where $\Omega^{NS,j}$ is given in (3.21), $V^{ss}(x)$ is given in (3.11), $\overrightarrow{V}^{ss}$ is given by (3.17), $\mathbb{I}$ is the identity matrix,

$$g_n^S(x,x_d) = \frac{\langle G^S(x,x_d), X_n(x)\rangle_A}{\langle X_n(x), X_n(x)\rangle_A},$$

and the $X_n(x)$ are given by (3.13).

As in the main paper, we can use (A.9) to solve for the bias current applied to the soma needed to bring the steady-state voltage at $x=0$ above 1,

$$I_{th} = G_L + \gamma\tanh(L) - I_d\frac{\gamma\cosh(L-x_d)}{\cosh(L)}. \tag{A.12}$$

Equation (A.12) is plotted in Figure 14 (a) as a function of x_d for different values of I_d. As I_d gets larger, I_{th} greatly decreases for proximal dendritic inputs. However, as the dendritic

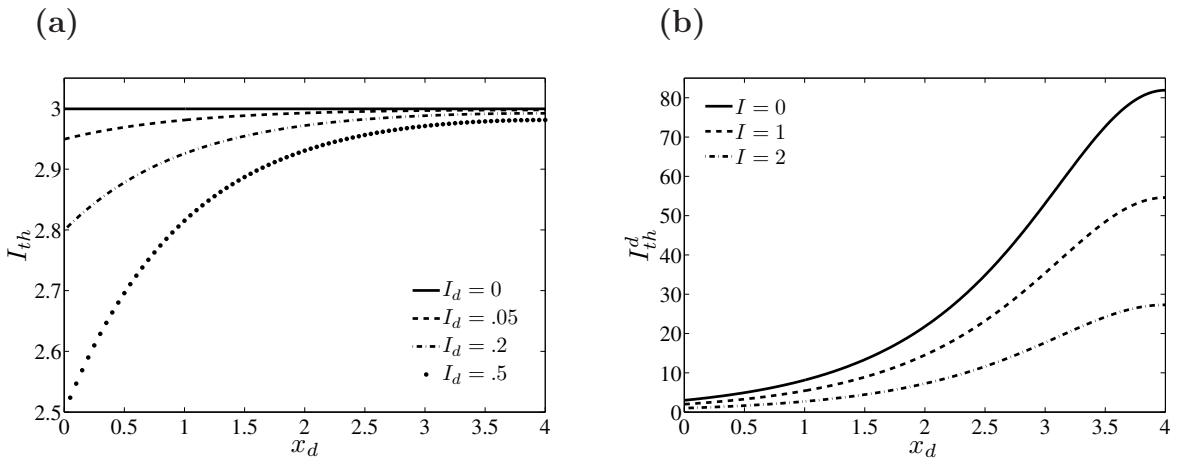

Figure 14. The position of the dendritic input affects both the somatic bias current and the dendritic input current needed to guarantee monostable firing. (a) *Somatic bias current needed to guarantee monostable firing* I_{th} (A.12) *plotted as a function of the position of the dendritic input* x_d *for four different values of the dendritic input current* I_d. (b) *Dendritic input current needed to guarantee monostable firing* I^d_{th} (A.13) *as a function of* x_d *for three different values of the somatic bias current* I. *In both figures,* $G_L = 2$, $\gamma = 1$, *and* $L = 4$.

input becomes more distal, I_{th} increases and reaches an asymptote that is close to the value when $I_d = 0$.

Similarly, we can solve for the dendritic point source input current needed to bring the steady-state voltage at $x = 0$ above 1,

$$I^d_{th} = \frac{\gamma \sinh(L) + (G_L - I)\cosh(L)}{\gamma \cosh(L - x_d)}. \tag{A.13}$$

I^d_{th} is plotted in Figure 14 (b) as a function of x_d for different values of I. Notice that, as the dendritic input becomes more distal, the value of I^d_{th} becomes very large. However, moderate increases in the somatic bias current act to greatly decrease the value of I^d_{th} even when the dendritic input is very distal.

Figure 15 plots the two bifurcation diagram for the somatic bias current versus the somatic spike height when $I_d = .2$ and the position of the dendritic point source input is varied. The figure shows that the bifurcation structure of the system with dendritic inputs is qualitatively similar to that of Figure 6 (a). Furthermore, the figure also reveals that the addition of the dendritic input acts to (i) decrease the amount of somatic bias current needed for monostable firing and (ii) cause the bifurcation to bistability to occur for smaller values of the somatic spike height. Point (i) occurs because the dendritic input causes the dendrite to source current to the soma when the voltage is subthreshold, thus allowing it to reach threshold with a lower bias current. Point (ii) occurs because, during the spike, both the soma and the dendrite are now sourcing current to the proximal dendrite causing it to become more depolarized and thus allowing the ping-pong effect to occur for smaller values of the somatic spike height. Note that this scenario can be different if the somatic dynamics during the spike are allowed to be

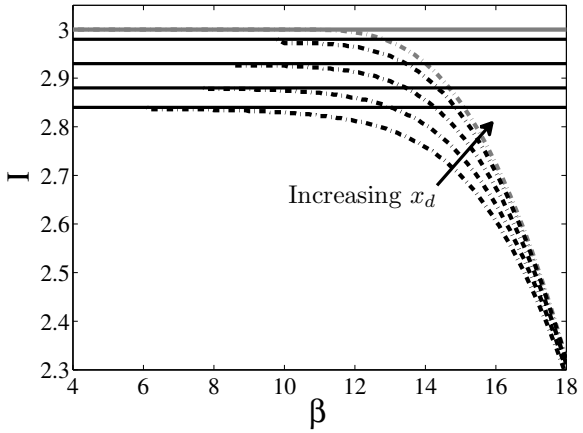

Figure 15. Dendritic inputs do not qualitatively affect the bifurcation structure. *Two parameter bifurcation diagram for the current applied to the soma I versus spike amplitude β (similar to Figure 6 (a)). As in the previous bifurcation diagrams, the solid line represents I_{th} (i.e., the curve in parameter space above which the quiescent solution does not exist) and the dash-dotted line represents the minimum amount of applied current needed to sustain oscillations via the ping-pong effect (i.e., the curve in parameter space where the stable oscillatory solution first coexists with the stable quiescent solution). The grey lines represent the bifurcation diagram when $I_d = 0$, while the black lines plot the bifurcation diagrams when $I_d = .2$ and x_d is (in order from lowest to highest) .2, .5, 1, and 2. In this figure, $G_L = 2$, $\gamma = 1$, $T_a = .2$, $V_R = -2$, and $L = 4$.*

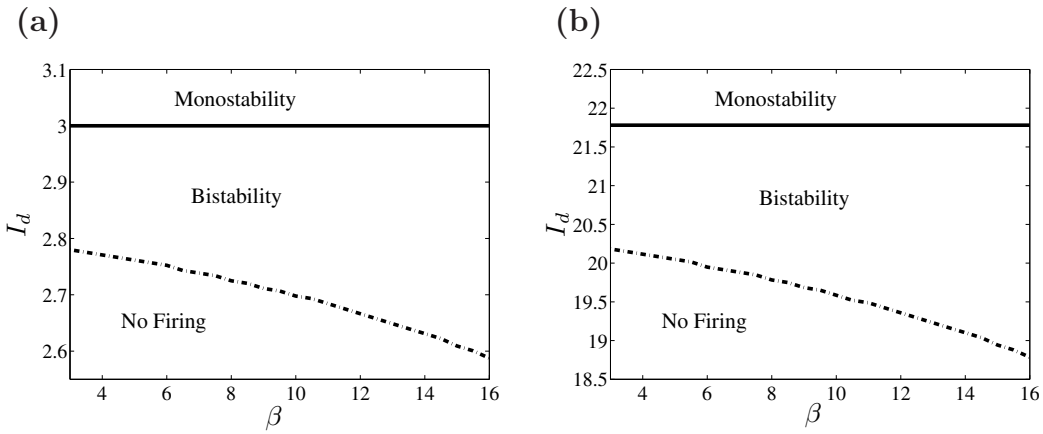

Figure 16. The ping-pong effect can occur with only dendritic input. *Two parameter bifurcation diagram for the dendritic point source input current I_d versus spike amplitude β when* (a) $x_d = 0$ *and* (b) $x_d = 2$ *and the somatic bias current is zero. Other parameters are the same as in Figure 15.*

affected by the dendritic dynamics and are not prescribed by a time-varying spike function as is the case in our model. As the dendritic input becomes more distal, the bifurcation structure of the system approaches that of the the system with no dendritic inputs, i.e., $I_d = 0$, which is plotted as the grey lines in the figure. Thus, dendritic inputs appear to not qualitatively affect the bifurcation structure of the system.

Finally, Figure 16 plots the two bifurcation diagram for the dendritic point source input

current I_d versus the somatic spike height when $I = 0$. The figures show that bistability can still occur in the system with current being applied only to the dendrite. Furthermore, as the dendritic input becomes more distal, the bifurcation diagram remains qualitatively the same and is only shifted upward.

Acknowledgment. The authors would like to thank Jiawei Zhang for comments on the manuscript.

REFERENCES

[1] L. F. Abbott, *Lapicques introduction of the integrate-and-fire model neuron* (1907), Brain Res. Bull., 50 (1999), pp. 303–304.
[2] A. Bose and V. Booth, *Bursting in 2-compartment neurons: A case study of the Pinsky-Rinzel model*, in Bursting: The Genesis of Rhythm in the Nervous System, S. Coombes and P. Bressloff, eds., World Scientific, New York, 2005, pp. 123–144.
[3] P. Bressloff, *Dynamics of a compartmental model integrate-and-fire neuron with somatic potential reset*, Phys. D, 80 (1995), pp. 399–412.
[4] P. C. Bressloff and S. Coombes, *Physics of the extended neuron*, Int. J. Mod. Phys. B, 11 (1997), pp. 2343–2392.
[5] F. S. Chance, L. F. Abbott, and A. D. Reyes, *Gain modulation from background synaptic input*, Neuron, 35 (2002), pp. 773–782.
[6] C. C. Chow and N. Kopell, *Dynamics of spiking neurons with electrical coupling*, Neural Comput., 12 (2000), pp. 1643–1678.
[7] R. V. Churchill, *Expansions in series of non-orthogonal functions*, Bull. Amer. Math. Soc., 48 (1942), pp. 143–149.
[8] S. M. Crook, G. B. Ermentrout, and J. M. Bower, *Dendritic and synaptic effects in systems of coupled cortical oscillators*, J. Comput. Neurosci., 5 (1998), pp. 315–329.
[9] B. Doiron, C. Laing, and A. Longtin, *Ghostbursting: A novel neuronal burst mechanism*, J. Comput. Neurosci., 12 (2002), pp. 5–25.
[10] D. Durand, *The somatic shunt cable model for neurons*, Biophys. J., 46 (1984), pp. 645–653.
[11] A. Erisir, D. Lau, B. Rudy, and C. S. Leonard, *Function of specific k+ channels in sustained high-frequency firing of fast-spiking neocortical interneurons*, J. Neurophysiol., 82 (1999), pp. 2476–2489.
[12] G. B. Ermentrout, *Type 1 membranes, phase resetting curves, and synchrony*, Neural Comput., 8 (1996), pp. 1979–1001.
[13] J. M. Fuster, *Memory in the Cerebral Cortex*, MIT Press, Cambridge, MA, 1996.
[14] A. L. Hodgkin, *The local electric changes associated with repetitive action in a non-medulated axon*, J. Physiol., 107 (1948), pp. 165–181.
[15] W. Holmes, *The role of dendritic diameters in maximizing the effectiveness of synaptic inputs*, Brain Res., 478 (1989), pp. 127–137.
[16] E. M. Izhikevich, *Dynamical Systems in Neuroscience: The Geometry of Excitability and Bursting*, MIT Press, Cambridge, MA, 2007, Chapter 10.
[17] R. Jolivet, T. J. Lewis, and W. Gerstner, *Generalized integrate-and-fire models of neuronal activity approximate spike trains of a detailed model to a high degree of accuracy*, J. Neurophysiol., 92 (2004), pp. 959–976.
[18] C. Koch, *Biophysics of Computation: Information Processing in Single Neurons*, Oxford University Press, New York, 1999.
[19] C. Koch and I. Segev, *The role of single neurons in information processing*, Nature, 3 (2000), pp. 1171–1177.
[20] C. Laing and A. Longtin, *A two-variable model of somatic-dendritic interactions in a bursting neuron*, Bull. Math. Biol., 64 (2002), pp. 829–860.
[21] P. Lánský and R. Rodriguez, *The spatial properties of a model neuron increases its coding range*, Biol. Cybernet., 81 (1999), pp. 161–167.

[22] T. J. Lewis and J. Rinzel, *Dynamics of spiking neurons connected by both inhibitory and electrical coupling*, J. Comput. Neurosci., 14 (2003), pp. 283–309.
[23] T. J. Lewis and J. Rinzel, *Dendritic effects in networks of electrically coupled fast-spiking interneurons*, Neurocomputing, 58–60 (2004), pp. 145–150.
[24] Z. F. Mainen and T. J. Sejnowski, *Influence of dendritic structure on firing pattern in model neocortical neurons*, Nature, 382 (1996), pp. 363–366.
[25] J. G. Mancilla, T. J. Lewis, D. J. Pinto, J. Rinzel, and B. W. Connors, *Synchronization of electrically coupled pairs of inhibitory interneurons in neocortex*, J. Neurosci., 27 (2007), pp. 2058–2073.
[26] C. Morris and H. Lecar, *Voltage oscillations in the barnacle giant muscle fiber*, Biophys. J., 35 (1981), pp. 193–213.
[27] F. Nadim and J. Golowasch, *Signal transmission between gap-junctionally coupled passive cables is most effective at an optimal diameter*, J. Neurophysiol., 95 (2006), pp. 3831–3843.
[28] P. F. Pinsky and J. Rinzel, *Intrinsic and network rhythmogenesis in a reduced Traub model for ca*3 *neurons*, J. Comput. Neurosci., 1 (1994), pp. 39–60.
[29] A. Prescott, S. Ratté, Y. De Kininck, and T. J. Sejnowski, *Pyramidal neurons switch from integrators in vitro to resonators under in vivo-like conditions*, J. Neurophysiol., 100 (2008), pp. 3030–3042.
[30] Y. Prut and E. E. Fetz, *Primate spinal interneurons show pre-movement instructed delay activity*, Nature, 401 (1999), pp. 590–594.
[31] W. Rall, *Membrane time constants of motoneurons*, Science, 126 (1957), p. 454.
[32] W. Rall, *Branching dendritic trees and motoneuron membrane resistivity*, Exp. Neurol., 2 (1959), pp. 491–527.
[33] W. Rall, *Membrane potential transients and membrane time constant of motoneurons*, Exp. Neurol., 2 (1960), pp. 503–532.
[34] W. Rall, *Theory of physiological properties of dendrites*, Ann. N.Y. Acad. Sci., 96 (1962), pp. 1071–1092.
[35] J. Rinzel and G. B. Ermentrout, *Analysis of neural excitability and oscillations*, in Methods in Neuronal Modelling: From Synapses to Networks, C. Koch and I. Segev, eds., MIT Press, Cambridge, MA, 1989, pp. 135–171.
[36] M. A. Schwemmer and T. J. Lewis, *Effects of dendritic load on the firing frequency of oscillating neurons*, Phys. Rev. E, 83 (2011), 031906.
[37] R. Traub, R. Wong, R. Miles, and H. Michelson, *A model of a ca*3 *hippocampal pyramidal neuron incorporating voltage-clamp data on intrinsic conductances*, J. Neurophysiol., 66 (1991), pp. 635–649.
[38] J. van Ooyen, A. Duijnhouwer, M. W. H. Remme, and J. van Pelt, *The effect of dendritic topology on firing patterns in model neurons*, Network: Comput. Neural Syst., 13 (2002), pp. 311–325.
[39] X. J. Wang, *Fast firing and short-term synaptic plasticity: A model of neocortical chattering neurons*, Neuroscience, 89 (1999), pp. 347–362.